NUMERICAL COMPARISON AND SIZING OF SENSIBLE AND LATENT THERMAL ENERGY STORAGE FOR COMPRESSED AIR ENERGY STORAGE

A THESIS SUBMITTED TO
THE GRADUATE SCHOOL OF NATURAL AND APPLIED SCIENCES
OF
MIDDLE EAST TECHNICAL UNIVERSITY

BY

MİNE KAYA

IN PARTIAL FULFILLMENT OF THE REQUIREMENTS
FOR
THE DEGREE OF MASTER OF SCIENCE
IN
MECHANICAL ENGINEERING

AUGUST 2015

Approval of the thesis:

NUMERICAL COMPARISON OF SENSIBLE AND LATENT THERMAL ENERGY STORAGE FOR COMPRESSED AIR ENERGY STORAGE

submitted by **MİNE KAYA** in partial fulfillment of the requirements for the degree of **Master of Science in Mechanical Engineering Department, Middle East Technical University** by,

Prof. Dr. Gülbin Dural Ünver
Dean, Graduate School of **Natural and Applied Sciences** _____

Prof. Dr. Tuna Balkan
Head of the Department, **Mechanical Engineering** _____

Assoc. Prof. Dr. İlker Tarı
Supervisor, **Mechanical Engineering Dept., METU** _____

Assoc. Prof. Dr. Derek K. Baker
Co-Supervisor, **Mechanical Engineering Dept., METU** _____

Examining Committee Members:

Assoc. Prof. Dr. Almıla Güvenç Yazıcıoğlu
Mechanical Engineering Dept., METU _____

Assoc. Prof. Dr. İlker Tarı
Mechanical Engineering Dept., METU _____

Assoc. Prof. Dr. Derek K. Baker
Mechanical Engineering Dept., METU _____

Asst. Prof. Dr. F. Nazlı Dönmezer Akgün
Mechanical Engineering Dept., METU _____

Prof. Dr. Ayhan Yilmazer
Department of Nuclear Engineering, Hacettepe University _____

Date: 06/08/2015

I hereby declare that all information in this document has been obtained and presented in accordance with academic rules and ethical conduct. I also declare that, as required by these rules and conduct, I have fully cited and referenced all material and results that are not original to this work.

Name, Last Name : _____

Signature : _____

ABSTRACT

NUMERICAL COMPARISON AND SIZING OF SENSIBLE AND LATENT THERMAL ENERGY STORAGE FOR COMPRESSED AIR ENERGY STORAGE

Kaya, Mine

M.S., Department of Mechanical Engineering

Supervisor : Assoc. Prof. Dr. İlker Tarı

Co-Supervisor : Assoc. Prof. Dr. Derek K. Baker

July 2015, 94 pages

Intermittent and variable characteristics of renewable energy systems can be compensated by energy storage systems (ESS). There is a wide range of ESS specialized for different applications. Compressed Air Energy Storage (CAES) is often used for wind power plants due to high power rating at the discharge and long discharge duration. CAES takes ambient air and pressurizes through a compressor and stores compressed air in a volume when supplied energy is greater than demand. If demand exceeds supply, CAES is discharged by drawing compressed air from storage, running turbine after heating compressed air by external heat source (fuel). Thermal Energy Storage (TES) is another ESS, which is generally coupled with solar thermal energy systems. TES systems can store sensible or latent heat in a storage medium. A feature of TES is capability of being used with CAES. External heat source can be eliminated by TES by storing thermal energy of air at the compressor exhaust to be

used to heat air before turbine. CAES with TES systems are named as Adiabatic CAES (A-CAES) and comprise of a compressor, TES, air storage and a turbine. In this study, TES of an A-CAES system is modeled and effect of TES on CAES is investigated. Performance of individual TES is analyzed for different heat storage mediums - latent and sensible -, tank and heat storage medium dimensions. Aim of the present study is to model a TES, which is capable of storing maximum heat in a minimum volume and shortest duration and implement the promising designs to CAES and investigate the performance of overall system by means of efficiency and total work output using MATLAB.

Keywords: Compressed Air Energy Storage, CAES, Thermal Energy Storage, TES, PCM

ÖZ

SIKIŞTIRILMIŞ HAVA ENERJİ DEPOSU İÇİN DUYULUR VE GİZLİ ISIL ENERJİ DEPOLARININ BOYUTLANDIRILMASI VE SAYISAL KARŞILAŞTIRILMASI

Kaya, Mine

Yüksek Lisans, Makina Mühendisliği Bölümü

Tez Yöneticisi : Doç. Dr. İlker Tarı

Ortak Tez Yöneticisi : Doç. Dr. Derek K. Baker

Ağustos 2015, 94 sayfa

Yenilenebilir enerji sistemtelerinin kesintili ve değişken yapıları, enerji depolama sistemleri (EDS) ile dengelenebilir. Farklı uygulamalar için kullanılabilecek çok sayıda EDS vardır. Sıkıştırılmış hava enerji deposu (SHED), yüksek güç seviyesi ve uzun çalışma saatleri nedeniyle genellikle rüzgar enerjisi sistemleriyle birlikte kullanılır. Enerji arzı yüksek, talep düşük olduğunda, SHED ortamdan aldığı havayı kompresörde sıkıştırarak hava deposunda saklar. Enerji talebi arzdan fazla olduğunda ise, SHED depoladığı havayı türbinde elektrik elde etmek üzere kullanır. Türbine giren havayı ısıtmak için harici bir ısı kaynağı kullanılır. Isıl enerji deposu (IED) genellikle güneş enerjisi sistemleri ile birlikte çalışır ve duyulur vey a gizlil ısı depolayabilir. SHED sistemlerinden harici ısı kaynağını çıkarmak için IED sistemleri kullanılabilir. IED kompresör çıkışındaki sıcak havanın ısıl enerjisini gerektiğinde yeniden kullanmak için depolar. IED barındıran SHED sistemleri Adiyabatik-SHED (A-SHED) olarak anılır ve kompresör, IED, hava deposu ve türbinden oluşur. Bu çalışmada, SHED sisteminde kullanılmak üzere IED tasarlanacak ve IED sisteminin

SHED üzerindeki etkisi araştırılacaktır. IED sistemi bireysel olarak incelenecek ve performansı üzerinde etkisi bulunan parametreler belirlenecektir. Bu çalışmanın amacı azami ısıyı asgari hacimde ve en kısa sürede depolayan bir IED sistemi tasarlamak ve bu sistemi SHED sistemine uygulamaktır. System peformansı MATLAB kullanarak verim ve toplam iş çıktısı açısından değerlendirilecektir.

Anahtar Kelimeler: Sıkıştırılmış Hava Enerji Deposu, Isıl Enerji Deposu, Faz Değiştirici Malzeme

To Ege and Bade

ACKNOWLEDGEMENTS

First, I would like to express my appreciation to my supervisor, Dr. İlker Tarı for his guidance and supervision throughout this thesis. He has been always kind and supportive throughout this study. I have also been grateful to my co-supervisor, Dr. Derek Baker for his invaluable contribution to my academic background and vision since I participated in ISEP 2011.

I want to thank to my big family for their endless love and support. I would not have been able to accomplish this work without them.

I would like to thank to my colleagues: Eylül for her friendship and our nice talks, to Serhat for his songs and friendship for eight years, my dear roommates Göker for those I learnt from him and especially for his immediate help at the end of my thesis and Erdem for his kindness, to Berke for cheering me up. I also want to thank to Mustafa Yalçın for our tea and coffee breaks. The best tea and coffee were made in our laboratory and with my dear friends.

Finally, I would like to express my special thanks to Onur for his comments, feedbacks and our invaluable discussions about this thesis. I also thank to him for making me happy for years.

TABLE OF CONTENTS

TABLE OF FIGURES

FIGURES

TABLE OF TABLES

TABLES

NOMENCLATURE

Abbreviations	
CAES	Compressed Air Energy Storage
ESS	Energy Storage Systems
FVM	Finite Volume Method
HTF	Heat transfer fluid
LHTES	Latent Heat Thermal Energy Storage
PCM	Phase Change Material
PHS	Pumped Hydro Storage
SHTES	Sensible Heat Thermal Energy Storage
TES	Thermal Energy Storage
Symbols	
A	Area
Bi	Biot Number
c	Specific heat
c_p	specific heat
D	Diameter
h	Convective heat transfer coefficient
h	Enthalpy
$J(T)$	Probability of crystallization
k	Conductivity Specific heat ratio
L	Length
L_c	Characteristic length
L_F	Latent heat of fusion
m	Mass
$\dot{m}$	Mass flow rate of the air
N	Number of capsules in a layer
$n(t)$	Number of capsules experiencing phase change
$n_f(t)$	Number of completely frozen capsules
Nu	Nusselt Number
$n_{unc}(t)$	Number of uncrystallized capsules at time t
P	Pressure
Pr	Prandtl Number
Q_{gain}	Heat gain
Q_{loss}	Heat loss

Q_{TES}	Stored Heat in TES
$\dot{q}$	Rate of heat exchange of individual capsules with HTF
$\dot{Q}$	Rate of heat exchange of all capsules in the layer with HTF
R	Ideal gas constant of air
r	Radius, radial
R	Thermal resistance
Re	Reynolds Number
r_p	Pressure Ratio
s	Entropy
S	Surface area of a capsule
t	time
T	Temperature
T_b	Temperature of heat transfer liquid in the layer
T_L	Homogeneous liquid PCM temperature
T_s	Homogeneous solid PCM temperature
u	Internal energy
V	Volume
v	Specific volume
$\dot{V}$	Volumetric flow rate
v_s	Superficial velocity
W	Work
$\dot{W}$	Power
Greek Letters	
$\Delta n(t)$	Number of capsules which is crystallized at time t
Δp	Pressure Drop
ΔT	Supercooling degree
ε	Porosity of the tank
η	Isentropic efficiency
ν	Kinematic viscosity
ρ	Density
τ	Moment of freezing starts first
Subscripts	
c	Crystallization, Compressor, Compression
cap	Capsule
e	Expansion
env	Envelope
eq	Equavalent
f	Convective
hyd	Hydraulic
i	inner

in	inlet
init	Initial
L	Liquid
lat	latent
lay	Layer
m	Melting
max	Maximum
min	Minimum
o	Outer, Ambient
out	Outlet
ref	reference
rev	reversible
s	Solid
sen	sensible
st	Air Storage
t	Turbine
tank	TES Tank
tot	Total
Superscripts	
s	Isentropic

CHAPTER 1

INTRODUCTION

1.1. Background

Energy demand has increased since industrial revolution. Energy has become one of the main necessities of modern world due to increase in the population, industrial and technological improvements and new types of electronic devices which come into our lives. Figure 1 represents this increasing trend. Total energy consumption has increased more than twice within 40 years. Even in the last two decades, energy consumption increased by approximately 40%.

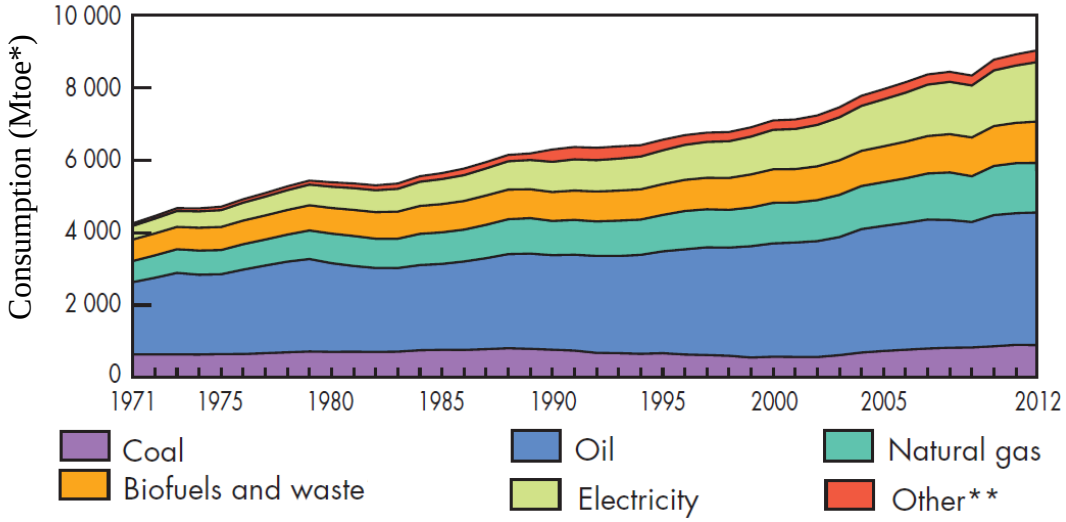

*Mtoe: million tons of equivalent oil
**Geothermal, solar, wind

Figure 1. World total energy consumption from 1971 to 2012 by fuel.[1]

Considering the increase in energy demand in Figure 1 and limited source of energy in the world, reasonable energy usage has become a necessity and load leveling has gained importance. Load leveling is the regulation of electricity demand and supply in order to continuously operate power plants at close to optimum conditions. In traditional power plants, load leveling is subject to predicted daily and seasonal energy demand [2] with known energy supply. However, along with the progress in renewable energy in the last decades, load leveling has become more challenging because in addition to energy demand, supply may be unpredictable. This is due to variable and intermittent characteristic of most renewable energy systems. Renewable energy systems can not provide constant power due to meteorological changes. For example, power output of solar thermal energy systems changes during a day with change in incident angle of Sun and may be lower than desired amount due to clouds. For wind turbines, supplied power varies with change in wind speed. To illustrate, in Figure 2, power production from wind turbines and electricity demand in Western Denmark are presented.

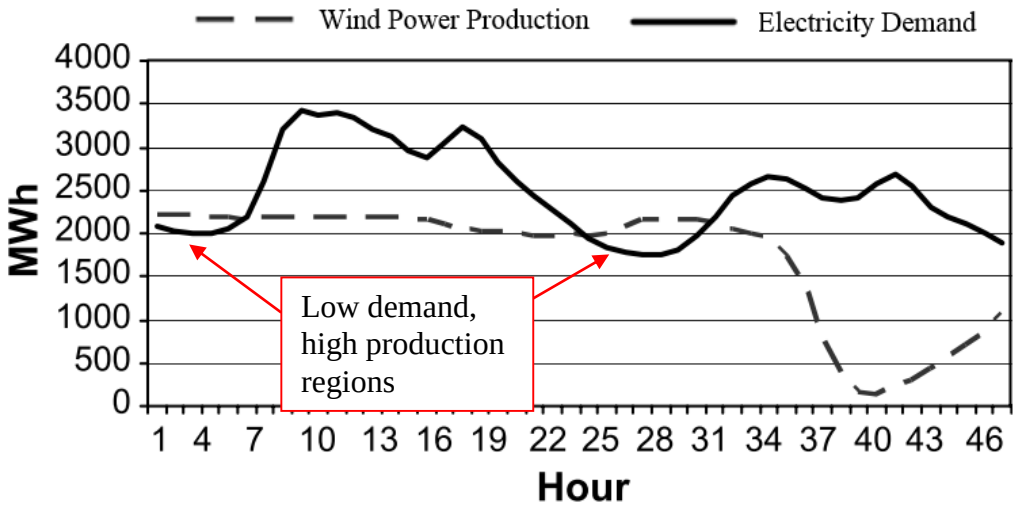

Figure 2. Example of net electricity demand and wind power production (Western Denmark on 07-08/01/2008) (Retrieved from [3]). Red arrows refer to potential of energy storage.

If an energy storage was established in Western Denmark, excess energy, which is shown with red arrows in Figure 2, might have been stored and contributed to the remaining time period, when the demand is higher.

Continuous operation need in renewable energy systems has accelerated the progress of energy storage. Therefore when electricity demand is lower than supply, storage system is charged and if the demand is higher, energy storage system is discharged for producing electricity.

1.2. Energy Storage

Electrical energy storage can be defined as a process of converting electrical energy to another form of energy which is storable and converting this another form again to electrical energy at a later time when necessary [4]. Chen *et al.* [4] reviewed the possible energy storage applications in traditional electricity value chain for load

leveling. Load leveling can be achieved by large (grid)-scale energy storage systems which can handle hours of operation and supply MW-scale power during discharge.

There is a variety of energy storage techniques which are classified according to the storage method, capacity and discharge rate. In Figure 3, energy storage systems are classified according to the storage method. Storage method indicates the form of stored energy, to which excess energy is converted. Electrical energy can be converted and stored in forms of mechanical, thermal, electrochemical energy or as electrical energy by means of capacitors.

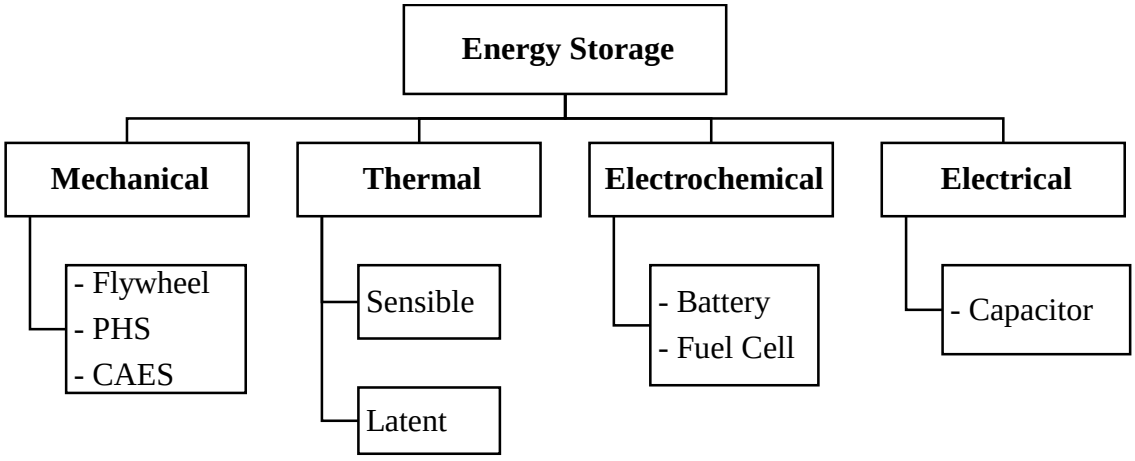

Figure 3. Classification of energy storage systems (ESS) according to form of stored energy (Adapted from [4], [5])

Mechanical energy can be stored by means of flywheels, pumped hydro storage (PHS) and compressed air energy storage (CAES). Flywheels stores rotational energy. During charging, a motor spins the flywheel and during discharge stored rotational energy is converted into electricity. Flywheels provide moderate-scale storage which are utilized in frequency regulation applications in critical applications [6]. PHS stores gravitational energy by the elevation change of storage medium during charging and discharging. CAES stores pressurized air and feeds turbine when electricity demand is

high. PHS and CAES are large-scale energy storage systems (ESS) which can handle the intermittency and variations of renewable energy systems. PHS and CAES systems will be investigated in more detail in Sections 1.2.1 and 1.2.2

Thermal energy storage system (TES) contains heat storage material which is heated or cooled during charging and discharging depending on the application. TES is applicable in a wide range of operations including domestic heating, cooling and solar power systems. Domestic cooling requires low temperature storage while heating or solar thermal energy require hot storage. TES systems may be used for both thermal energy like HVAC applications or may be contributed to electricity production as an auxiliary system in solar thermal energy systems.

Electrochemical storage systems include batteries, fuel cells and electrolyzers. Batteries are the oldest form of electricity storage [4]. Since first invented, batteries have been one of the most widely used ESS. There are different types of batteries, e.g. lead acid, sodium sulphur, sodium nickel, and lithium-ion. Fuel cells can produce electricity from fuel and oxidant. When excess electricity is available, electrolyzers can generate fuel and oxidant to be used when demand is higher. Electrochemical storage systems cover a wide range of applications from small electronic devices to cars, which can be respectively classified as low and moderate-scale energy storage systems.

Direct storage of electricity can be achieved with capacitors which consist of two metal plates and a dielectric separating the metal plates. A capacitor can be charged faster than batteries but provides power at very small rates.

ESS technologies are often classified based on their power ratings and discharge times. Power rating refers to power output during discharge and discharge time refers to how long ESS can generate power. ESS may be classified as uninterruptable power supply (UPS), grid support and bulk power management according to power ratings. Large scale ESS requires both high power ratings and long discharge times. In Figure 4, classification of ESS based on power rating and discharge times is presented.

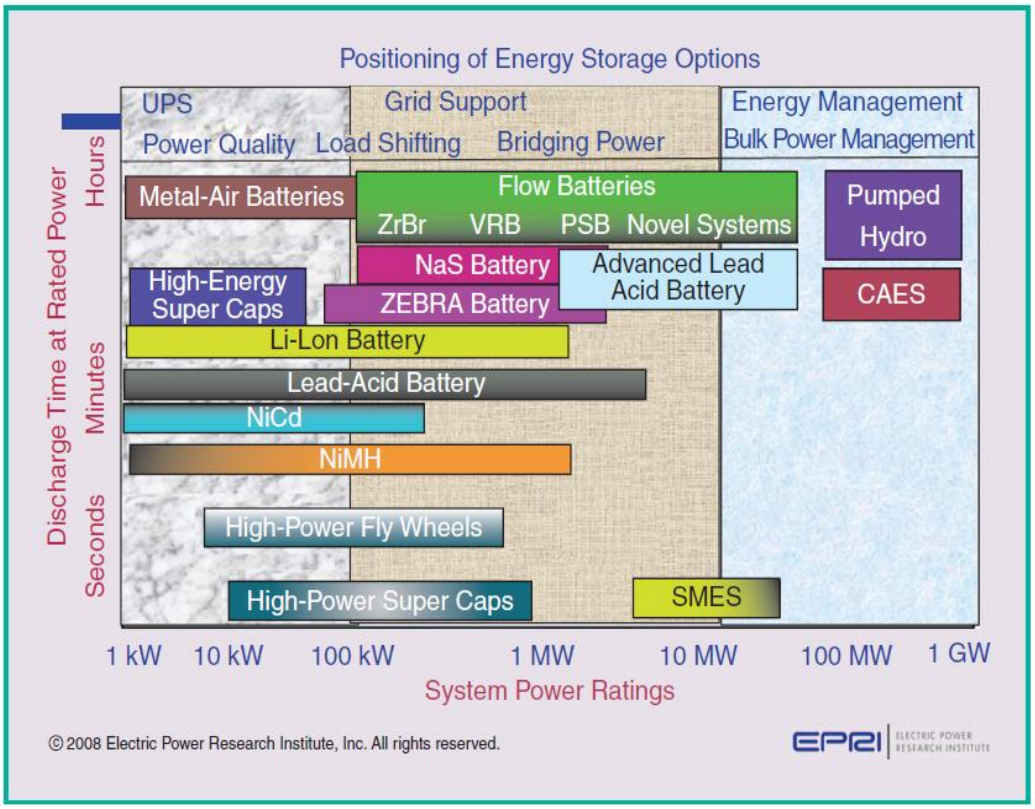

Figure 4. Comparison of ESS according to power rating and discharge time (Retrieved from [7]).

According to Figure 4, only PHS and CAES provide large-scale energy storage. The focus of this study is large-scale energy storage therefore PHS and CAES are discussed in Sections 1.2.1 and 1.2.2 in detail.

1.2.1. Pumped Hydro Storage (PHS)

In pumped hydro storage (PHS), electricity is stored as potential energy by pumping water to an elevated place, called upper reservoir. PHS is one of the widely used Large Scale ESS. Worldwide PHS capacity was around 100 GW by 2012 [4].

In Figure 5, operating principle of PHS is presented. PHS contains two reservoirs, upper and lower, and a turbine/pump. When electricity demand is low, turbine operates

as a pump and water is stored in upper reservoir and when supplied electricity is not sufficient, potential energy of water stored in the upper reservoir is converted to electricity by running the turbine.

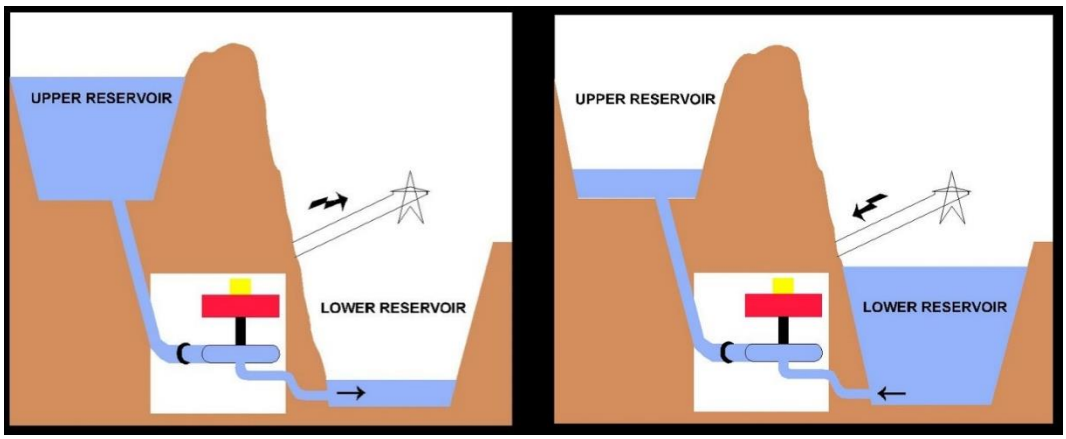

Figure 5. Operation principle of a pumped hydro storage facility. Discharge (left) and charge (right) durations (Retrieved from [8]).

PHS systems have the advantage of using water, which is one of the most common materials in world. However, high dependence on geography is a strong disadvantage of PHS. PHS system requires a location where an upper and a lower reservoir are available and this location should be near a power plant.

1.2.2. Compressed Air Energy Storage (CAES)

Another large scale ESS is CAES. CAES is based on working principle of gas turbines with the addition of an air storage volume. When excess energy is available, ambient air is compressed to high pressure and stored in the air storage. When electricity demand exceeds the supplied power, compressed air is used to drive turbine and generate power. In Figure 6, components of a CAES system are presented.

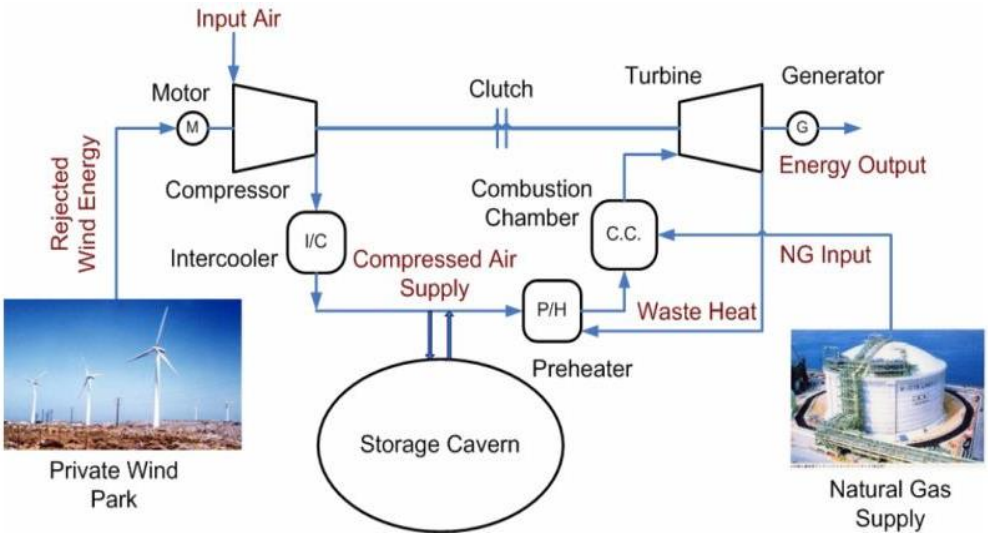

Figure 6. General representation of a CAES plant (Retrieved from [9]).

CAES plants are examined in subcategories according to the method of heating air before the turbine:

a. *Diabatic CAES (D-CAES):* Diabatic CAES refers to the conventional CAES systems which use a combustion chamber to reheat air before expansion as illustrated in Figure 6. The first two CAES facilities, Huntorf at Bremen, Germany and McIntosh at Alabama, USA are examples of D-CAES plants [10].
b. *Adiabatic CAES (A-CAES):* Adiabatic CAES is facilitated by eliminating the combustion chamber and introducing thermal energy storage (TES). During charging, hot air from the compressor exhaust is used to heat the storage medium and during discharging, the storage medium is used to heat air before entering the turbine.
c. *Isothermal CAES (I-CAES):* Isothermal compression or expansion is practically impossible; however, temperature change during compression or expansion can be lowered, which is called quasi-isothermal process. I-CAES systems are commercialized by several companies[11]–[13]. In I-CAES, water

piston, which comprises of water inside piston cylinder, is generally used. As the air is compressed, water absorbs heat. During expansion, process is reversed. High density and specific heat of water keeps temperature difference during compression and expansion small.

CAES and PHS provide similar storage capacities and both are dependent on geography. Geographical properties of desired site of installation is an important factor. For example, CAES is more suitable for the geography of USA [14], however, PHS may be more suitable for a different place. On the other hand, CAES is a relatively cheap application compared to PHS. In Figure 7, power rating and stored energy are presented for 1 yen (US $ 0.01) of capital cost. CAES stores higher amount of energy and provides higher power during discharge per unit cost.

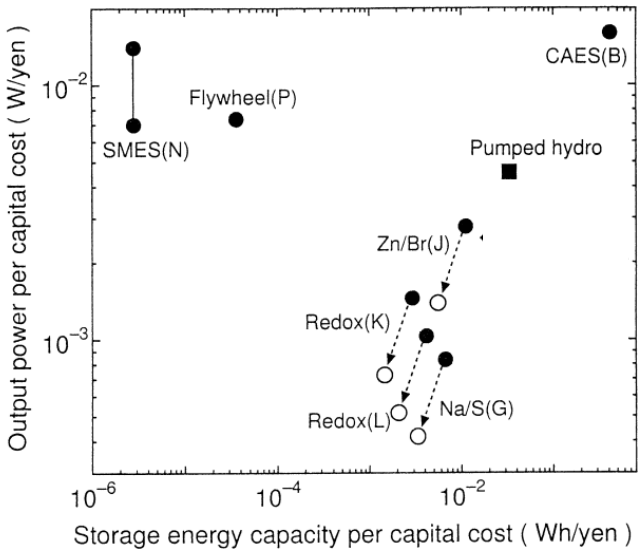

Figure 7. Output power and energy storage density per capital cost (100 yen = US $ 1) (Retrieved from [15]).

However, fuel usage in CAES systems should be completely eliminated to achieve a renewable ESS. Elimination of fuel can be achievable with further improvements in A-CAES and I-CAES systems. These improvements will be achieved with the progress in thermal energy storage.

1.2.3. Thermal Energy Storage

Thermal energy storage (TES) has a wide range of applications including solar thermal energy systems, residential heating and cooling, and combustion turbine inlet air cooling [16]. There are two types of TES, called sensible heat thermal energy storage (SHTES) and latent heat thermal energy storage (LHTES).

Sensible heat is stored by means of changing the temperature of a substance. An efficient SHTES can be achieved with materials of high density and high specific heat therefore gases are not preferred. Liquid water is commonly used in SHTES systems due to its low price and high specific heat, but has a limited operating temperature range (0-100 ^{0}C). Molten salts, bed rock [5] and concrete blocks are widely used solids in SHTES.

Latent heat is the energy transferred to/from the substance during phase change. LHTES utilizes latent heat. LHTES provides nearly isothermal heat storage on account of that the heat transfer medium remains at almost constant temperature during phase change. Substances which are used in LHTES are named as phase change materials (PCMs). Generally solid-liquid rather than liquid-gas phase change is preferable because volume change of substances is considerably high in liquid-gas phase change [5].

Due to the nearly-constant temperature heat storage, LHTES is more advantageous than SHTES. Table 1 presents a comparison of materials used in SHTES and LHTES.

Table 1. Comparison of various heat storage materials (Temperature change for sensible heat storage: $\Delta T = 15$ K) (Adapted from [17])

Heat Storage Materials		Sensible Heat TES		Latent Heat TES	
		Rock	**Water**	**Organic**	**Inorganic**
Latent Heat of Fusion	**kJ/kg**	-	-	190	230
Specific Heat	**kJ/kg**	1	4.2	2	2
Density	**kg/m^3**	2240	1000	800	1600
Storage mass for storing 10^6 kJ	**kg**	67000	16000	5300	4350
Storage volume for storing 10^6 kJ	**m^3**	30	16	6.6	2.7

Table 1 shows that, same amount of heat is stored in an approximately five times larger volume using water compared to inorganic PCM.

This study focuses on LHTES and aims to model a LHTES operating with CAES and compare LHTES with SHTES. In order to design a proper LHTES, PCMs should be examined in terms of physical and chemical behaviors. PCMs are discussed in detail in Section 1.2.3.1 in terms of their classification, advantages and disadvantages.

1.2.3.1. Phase Change Materials (PCMs)

One of the most important design parameters for LHTES is the melting temperature of PCM. Melting temperature specifies the proper operation condition. PCMs cover a wide melting temperature range.

PCMs are classified according to their thermal and chemical behavior [5] as presented in Figure 8.

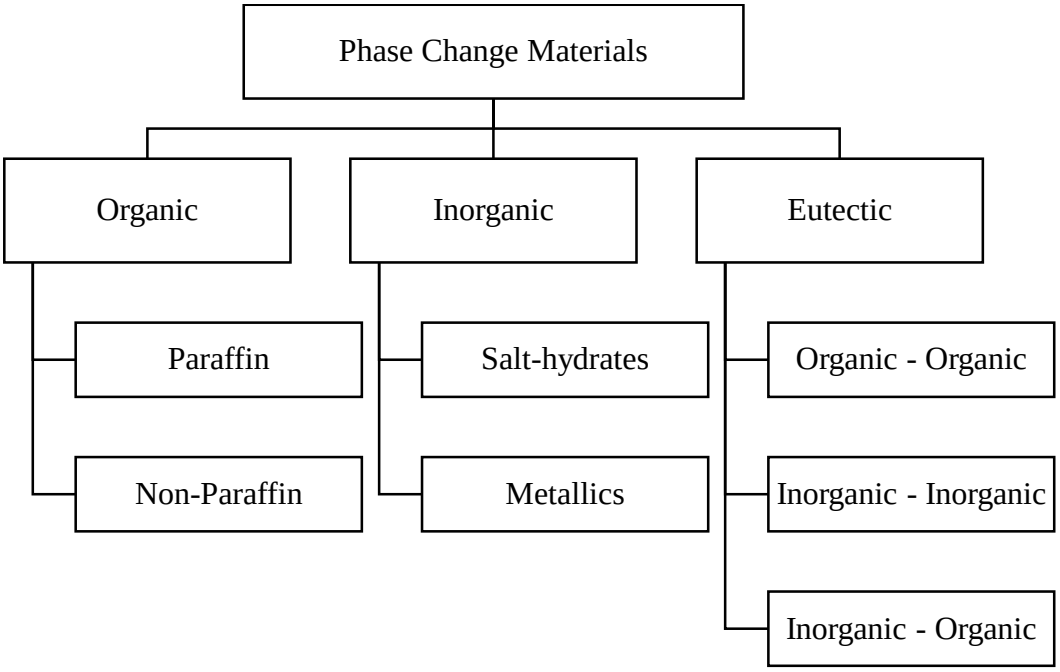

Figure 8. Classification of PCMs (Adapted from [5])

There are several problems associated with PCMs which affect the performance of LHTES. First, freezing has a stochastic nature in contrast with melting. Although melting starts at melting temperature, freezing may start at different temperatures below melting point. This phenomenon is called supercooling. As PCM is cooled below melting temperature without experiencing freezing, performance of LHTES decreases because if supercooling degree is high, process can be finished without latent heat is stored. In order to eliminate the effect of supercooling, researchers [18] suggested to use nucleating agents which make initiation of freezing easier. Furthermore non-toxicity and non-corrosivity are important for PCMs when selecting materials which are in contact with them[18]. Incongruent melting is another important problem if PCM is a solution. Incongruent melting occurs if solute is not completely soluble in melting at melting point and results in loss of performance [5].

PCM types in Figure 8 have different advantages and disadvantages as shown in Table 2. Among these PCMs, salt hydrates seems promising; however, incongruence and supercooling problems should be solved.

Table 2. Advantages and disadvantages of PCMs [5], [19]

	Advantages	Disadvantages
Organic		
Paraffin	• Congruent melting • Not corrosive	• Low thermal conductivity • Moderately flammable
Nonparaffin	• High heat of fusion	• Low thermal conductivity • Varying toxicity level • Flammability
Inorganic		
Salt Hydrates	• High latent heat per volume • High thermal conductivity • Small volume changes on melting • Inexpensive	• Incongruent melting • Supercooling

1.3. Recent Studies

The first CAES system was implemented in Huntorf, Germany in 1978. Huntorf has a 290 MW power capacity and maximum storage pressure of 70 bars. Later, McIntosh, Alabama plant was installed in 1991 with a power capacity of 110 MW and 78 bars of maximum storage pressure. Efficiency of a CAES system is the ratio of total work output of turbine to the sum of the work input for the compressor and the amount of electricity that could have been obtained from fuel input [14]. Efficiency of Huntorf plant is about 42 % while that of McIntosh is about 54% [20]. The efficiency of a CAES plant may be increased with elimination of fuel usage.

Huntorf and Alabama CAES plants have led the way to recent developments of CAES technology. In 2012, General Compression completed the third CAES project of the World which is quasi-isothermal CAES. The General Compression Advanced Energy Storage (GCAES™) system was built in Gaines, Texas in order to compensate the intermittency of wind power plant without fuel usage. In this system, excess power is stored in terms of high-pressure air and warm water [11] which is combination of compressed air and thermal energy storage. The EU-funded project ADELE is expected to be the first adiabatic CAES plant and planned to be constructed in Germany in 2017 [21]. The system is similar to existing D-CAES plants regarding air storage, compressors and turbines except the thermal energy storage is included. In order to achieve adiabatic storage, cylindrical structures made of pre-stressed concrete TES are utilized [22].

There are several studies investigating the thermodynamic performance of CAES. Zhang *et al.* ([23], [24]) investigated the performance of CAES systems thermodynamically. In the first study [23], effect of TES and number of compression and expansion stages on CAES performance are investigated. In the other study [24], authors analyzed different air storage models and proposed different methods for mathematical modeling. Hartmann *et al.* [25] also analyzed the performance of adiabatic CAES by simulating different configurations. In this study, the effects of number of compression stages and the differences between adiabatic and isothermal compression are investigated. Kim [26] performed a comprehensive study about novel CAES systems and analyzed these systems in terms of energy and exergy. The author proposed novel applications, e.g. utilizing CAES including micro-CAES system for heating and cooling purposes, CAES system combined with PHS. In these studies, no detailed design for the TES to be used is presented.

The studies ([23]–[26]) analyzed CAES systems in terms of thermodynamic performance only. Design of a TES including heat transfer analysis is not covered in these studies. However, to design an A-CAES system, TES should be carefully

designed and comprehensive understanding of heat storage characteristics is necessary.

Taştankaya [27] previously conducted a study based on CAES. In this study, an adiabatic CAES system with packed bed thermal energy storage was designed in order to compensate fluctuations in power produced by DARES Wind Farm in Datça, Turkey. Only single stage compression and expansion were utilized in the design and thus temperature at the exit of the compressor is too high, which can not be achieved by commercial compressors. Steta [28] studied the optimal operation strategies of CAES. Steta designed a CAES with a compression train of four intercooled compressors, a fixed-size TES made of concrete blocks (sensible heat storage), constant-volume air storage and an expansion train of two reheated turbines. A-CAES systems are not studied thoroughly except Taştankaya [27], Steta [28] and EU-funded ADELE [21] project. These studies covered only sensible heat TES and latent heat TES has not been considered for CAES.

1.4. Motivation of the Study

The present study focuses on the intermittency problem of renewable energy, mainly wind energy systems, which can be overcome by energy storage systems. Large-scale energy storage applications provide a solution of intermittency problem.

Among the grid-scale energy storage applications, CAES is more promising than PHS due to higher power rating and storage capacity per unit cost. However, for a completely renewable CAES system, TES should be implemented to CAES. TES design is a critical part of CAES and the most suitable design should be implemented.

Analyses of different types and configurations of TES systems have been presented in literature. However, there are limited number of studies on implementation of TES in CAES. Existing studies ([27], [28]) investigated utilization of sensible thermal energy storage in CAES. Utilization of LHTES in CAES has not been investigated yet.

1.5. Objective and Scope of the Study

In this study, CAES with a LHTES is studied. Objectives of this study are:

- Modeling of a Latent Heat Thermal Energy Storage (LHTES)
- Validation of LHTES model with experimental results in the literature.
- Comparison of some Phase Change Materials (PCMs) and sensible heat storage material (rock) to utilize in TES in terms of heat storage capacities and storage durations.
- Investigation of the effects of sizes of PCM capsules and TES tank on pressure drop.
- Modeling of the compression and expansion stages and air storage of CAES.
- Comparison of PCM-filled and rock-filled TES systems in terms of performance of CAES.

1.6. Thesis Organization

This study analyses CAES and TES systems and determines sizes of these. In the present study, there are four chapters.

In Chapter 2, mathematical model of TES is constructed and validated with an experimental study in the literature. A parametric study is conducted in order to investigate the effects of different PCMs and sensible thermal energy storage material rock, in different sizes of TES tank and capsules, on stored heat, storage duration and pressure drop.

In Chapter 3, compressor, turbine and air storage of CAES are modeled. Effects of different parameters on CAES model are investigated. An illustrative case is considered for the performance assessment of CAES with TES filled with different materials. CAES is three-stages and different sensible and latent heat storage mediums are analyzed in this system.

In Chapter 4, the present study is summarized briefly. Some conclusive remarks and future work are presented.

CHAPTER 2

MODELING OF LATENT HEAT THERMAL ENERGY STORAGE

2.1. Introduction

In this chapter, the mathematical model of a LHTES is presented. LHTES is a tank filled with encapsulated PCM. Encapsulation refers to the proper containment of PCMs. There are several different encapsulation methods, such as flat plates, shell and tube with parallel and cross flow, and sphere [29]. In this study, spherical capsules are modeled because of high heat transfer area-to-volume ratio and ease of implementation in almost all tank designs.

A simple schematic of LHTES system is given in Figure 9.

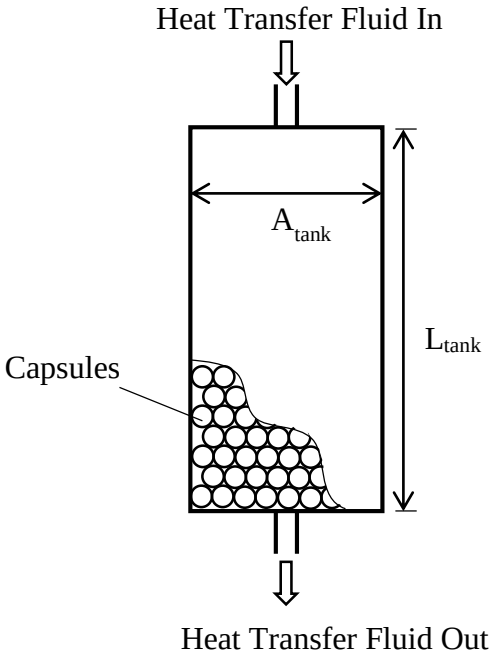

Figure 9. Schematic of a TES tank

HTF enters from one end of the LHTES and travels to the other end of the TES tank meanwhile heat is transferred to or from TES according to the temperature of PCM and HTF. LHTES can be used for cold or hot storage in different applications. Storage finishes when outlet temperature of HTF reaches to inlet temperature.

In this Chapter, mathematical model of LHTES is presented. Mathematical model will be verified using experimental data in literature. Effects of sizes of tank and capsules, and different types of heat storage mediums on stored heat, storage duration and pressure drop are investigated. The present model provides the flexibility to cover sensible storage model therefore comparison of LHTES and SHTES is done with the same mathematical model.

In this study, main focus is LHTES therefore TES refers to LHTES. SHTES is referred as its full abbreviation.

2.1. Mathematical Model

Mathematical modeling includes two sub-sections, modeling of capsules and modeling of the tank. Central differencing and explicit schemes of Finite Volume Method (FVM) are used for volume and time discretization.

Governing equations for capsule model include transient energy equation. The energy equation is discretized and temperature inside capsules is calculated for each time step. Total heat transfer from/to capsules due to the temperature difference between HTF and PCM is found with capsule model and used to calculate temperature of the HTF in tank model.

Tank is divided to a finite number of cells, called layers. The layers include the same number of capsules. Temperature of HTF inside layers is assumed as uniform. Energy equation of HTF is discretized for volume and time and temperature of the HTF is calculated at a specific location inside tank and time.

LHTES model provides information about stored heat which is the summation of heat exchange by each capsule throughout the process and temperature distribution inside LHTES tank.

Time step and cell lengths changes for each analysis in the present study.

2.1.1. Modeling of the Capsules

PCM capsules behave like heat exchanger. Heat transfer analysis differs according to the state of the PCM inside capsules. PCM may be completely-liquid, mixture of liquid and solid phases of PCM and completely-solid. Completely liquid and completely solid states have the same governing equations except the properties of the matter inside capsules. Melting and freezing of PCM occur during heating or cooling PCMs respectively which can refer to charging or discharging or vice versa. These two conditions are treated similarly except supercooling in freezing. In all cases, the

problem is pure conduction inside and forced convection at the outer surface of capsules.

During phase-change, process can be considered as the conduction problem in a spherical composite wall. Similar with the Stefan's analytical solution [30] for the phase change, during melting, solid is assumed to be at melting temperature and temperature of liquid changes. Similarly, during freezing, liquid is assumed at melting point and temperature of solid changes. Thermal resistances of walls (liquid during melting, solid during freezing and encapsulation material) can be used in order to determine heat exchange between PCM capsules and HTF. The aim of the analysis is to determine the heat transfer to or from HTF therefore exact solution of temperature distribution inside PCM is not required. Schematic of the capsules during phase change period is presented in Figure 10.

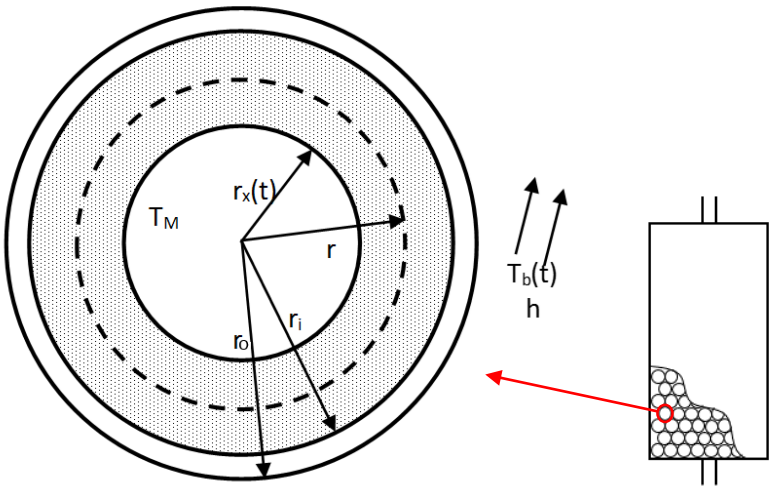

Figure 10. Schematic of the capsules during phase change. x is either L or C standing for liquid and crystal depending on the process, freezing or melting.

Completely-solid or completely-liquid condition cannot be simplified using thermal resistance approach because this approach is for walls. There is an exact solution for conduction through a sphere; however, the solution includes simple boundary conditions as constant wall temperature or heat flux. Lumped capacitance assumption is a possible approach for a full sphere.

Validity of lumped capacity assumption is checked by Biot number. Biot number is a dimensionless number which determines the dominant mode of heat transfer in transient problems and is defined simply as $Bi = h L_c / k$ where h is the convective heat transfer coefficient, L_c is the characteristic length and k is the thermal conductivity of body. For a sphere, characteristic length is one third of its outer radius; therefore Biot number for a sphere is[31]:

$$Bi = \frac{h r_o}{3k} \text{ where } k = k_L \text{ or } k = k_s \tag{1}$$

In this study, a wide range of different parameters are used therefore lumped capacitance assumption may not always be valid. Xu *et al.* [32] suggested an effective convective heat transfer coefficient for large Biot number applications. Effective heat transfer coefficient, h_{eff} is defined for a sphere as

$$h_{eff} = \frac{1}{\frac{1}{h} + \frac{r_o}{5k}} \tag{2}$$

where h is the actual heat transfer coefficient, r_o is the outer radius of PCM capsules and k thermal conductivity of solid or liquid PCM.

2.1.1.1. Completely Liquid or Solid inside Capsules

Heat exchange between capsules and HTF and homogeneous temperature of liquid and solid PCM is given below.

$$\dot{q}_x(t) = \frac{T_x(t) - T_b(t)}{R_f + R_{env}} \tag{3}$$

$$\rho_x c_x V_{cap} \frac{dT_x(t)}{dt} = -\frac{T_x(t) - T_b(t)}{R_f + R_{env}} \tag{4}$$

x is "*L"* or "*s"* according to the state of PCM inside capsules.

where

T_L and T_s are homogeneous liquid and solid PCM temperatures respectively.

T_b is the temperature of heat transfer liquid in the layer.

R_f and R_{env} are thermal resistances due to convection and envelope thickness respectively.

ρ_L, ρ_s, c_L and c_s are density and specific heat capacity of liquid and solid phase of PCM respectively.

V_{cap} is the volume of a capsule.

R_f and R_{env} are thermal resistances due to convection and envelope thickness respectively.

Convective resistance is defined as

$$R_f = \frac{1}{hS} = \frac{1}{h(4\pi r_o^2)} \tag{5}$$

S is surface area of a capsule.

Heat transfer coefficient can be found using appropriate formulation. Nusselt number can be determined from Equation (6) [33]:

$$Nu = \frac{hD_{hyd}}{k} = C\,\mathrm{Pr}^{1/3}\,\mathrm{Re}^{1/2} \tag{6}$$

where D_{hyd} is the hydraulic diameter of the tank: $D_{hyd} = \frac{2}{3} D_{eq} \frac{\varepsilon}{1-\varepsilon}$ where ε is the porosity of the tank and D_{eq} is the equivalent diameter of capsules and defined as $D_{eq} = 2r_o$

C is the constant which takes different values according to the process. Reynolds number is determined based on superficial velocity [34] of the HTF found by Equation (7).

$$\mathrm{Re} = \frac{v_s D_{eq}}{\nu(1-\varepsilon)} \tag{7}$$

Superficial velocity is the flow velocity which can be obtained in the same tank without capsules and defined as $v_s = \dot{V} / A_{\tan k}$

ν is the kinematic viscosity of the fluid.

However, if Biot number is lower than 0.1, convective heat transfer coefficient is replaced by effective heat transfer coefficient.

Thermal resistance due to the thickness of the envelope of capsules:

$$R_{env} = \frac{1}{4\pi k_{env}} \left(\frac{1}{r_i} - \frac{1}{r_o} \right) \tag{8}$$

k_{env} is the conductivity of envelope material.

2.1.1.2. Melting of PCM inside Capsules

Just before melting begins, temperature of the solid inside capsules reaches to T_m. After that moment, a liquid layer is formed and the remaining solid PCM is assumed to be at T_m throughout melting.

Heat transfer during melting can be expressed as

$$\dot{q}_m(t) = \frac{T_m - T_b(t)}{R_f + R_{env} + R_L(t)} \tag{9}$$

T_m is the melting temperature of the PCM.

$R_L(t)$is the thermal resistance due to the liquid layer formed during melting respectively.

$$R_L(t) = \frac{1}{4\pi k_L}\left(\frac{1}{r_L(t)} - \frac{1}{r_i}\right) \tag{10}$$

$r_L(t)$ is the inner radius of the liquid layer formed in the capsules due to melting. Solid PCM is assumed to start to melt from the inner surface of the capsule envelope and a liquid layer is formed. This liquid layer grows concentrically to the center of the capsule and melting is completed when $r_L(t)$ approaches to zero. If an infinitesimal element located at the solid-liquid interface is considered,

$$4\pi r_L^{\,2}(t)\rho_L L_F dr_L(t) = \dot{q}_m(t)\,\mathrm{dt} \tag{11}$$

$r_L(t)$ is equal to r_i just before melting starts and approaches to zero at the end of melting.

$$\text{PCM is} \quad \begin{cases} \text{completely-solid} & \text{if } T_s < 0°C \\ \text{liquid-solid mixture} & \text{if } T_s \approx 0°C \ \& \ 0 < r_L(t) \\ \text{completely-liquid} & \text{if } r_L(t) \approx 0 \end{cases}$$

According to the state of the PCM inside capsules, total heat transfer to the capsules becomes:

$$\dot{Q}(t) = N\left[\dot{q}_s(t) + \dot{q}_m(t) + \dot{q}_L(t)\right] \tag{12}$$

N is the total number of capsules in the corresponding control volume (layer). Because the states are strictly differentiated, at a specific time step there can only be one kind of heat transfer, sensible (liquid, solid) or latent.

2.1.1.3. Freezing of Capsules

Freezing process is different than melting. Although melting begins at exactly melting temperature, substance generally undergoes supercooling and freezing is initiated at a lower temperature than melting temperature. There are several substances, called nucleating agents, which lowers the supercooling degree [18]; however, it is difficult to completely eliminate supercooling. This phenomenon has not been widely studied in terms of mathematical modeling. Bedecarrats [35] developed a mathematical model for supercooling of water. However, supercooling characteristics of other PCMs have not been studied. In this study, behavior of water under supercooled condition is assumed to be valid for other PCMs. Bedecarrats' study indicates that capsules start to freeze at different times due to the stochastic character of freezing. Although capsules behave together during melting, they start to freeze at different times. A group of capsules may start to freeze although remaining capsules are still liquid. Capsules in a group exhibit same behavior regarding supercooling degree, start and end times of freezing.

In this study, freezing and crystallization means same. The term freezing is mostly used in the present study but Bedecarrats' terminology of crystallization is sometimes used.

During freezing of capsules, phenomenon is the reverse of melting. Heat transfer from the capsules:

$$\dot{q}_c(t) = \frac{T_m - T_b(t)}{R_f + R_{env} + R_c(t)} \tag{13}$$

Thermal resistance due to the thickness of the solid PCM layer is

$$R_c(t) = \frac{1}{4\pi k_s}\left(\frac{1}{r_c(t)} - \frac{1}{r_i}\right) \tag{14}$$

And the radius of solid layer is

$$4\pi r_c^{\,2}(t)\rho_s L_F\, dr_c(t) = -\dot{q}_c(t)\,\mathrm{dt} \tag{15}$$

Different than melting process, just before freezing, temperature of the liquid PCM is T_L and after freezing begins, a thin solid layer forms adiabatically (very rapid process) and temperature of liquid PCM increases to its constant melting temperature, T_m. Therefore, at the beginning of freezing period, there is an initial solid layer which can be expressed as

$$r_{init} = \left[r_i^3 \left(1 - \frac{\rho_L c_L}{\rho_s L_F} \Delta T \right) \right]^{1/3} \tag{16}$$

where ΔT is supercooling degree, $\Delta T=T_m-T_L(\tau)$

Supercooling [36] can be defined as the difference of the temperature of the liquid PCM at the beginning of the freezing than melting temperature. Supercooling cannot be eliminated but can be lowered using nucleating agents which accelerates the initiation of freezing. Therefore, solid formation does not start at a specific temperature but at variety of temperature below melting temperature.

Bedecarrats [35] developed a mathematical model based on experimental results to determine the beginning of freezing in a 30-L tank filled with 32 PCM capsules filled with water as PCM. He proposed a function called probability of crystallization of a capsule per unit of time, *J(T). J(T)* depends on homogeneous liquid temperature inside capsules, $T_L(t)$ and is formulated empirically as

$$J(T) = C_1 \exp\left[-\frac{C_2}{T(T_M - T)^2} \right] \tag{17}$$

C_1 and C_2 are 7.029 h^{-1} and 8350 K^3 respectively [35].

Number of new crystallizations during a finite time step is determined using $J(T_L)$.

$$\Delta n(t) = J\left(T_L(t)\right)\left(N - n(t)\right)\Delta t \tag{18}$$

The first time when Δn is greater than zero is the beginning of freezing, $t=\tau$.

If Δn is non-integer, probabilistic approach takes place. The greatest integer less than Δn is taken. And X is calculated by subtracting this integer from actual Δn value. r is a random number between 0 and 1, X is compared with r. If X is below r, new crystallization is (Δn_τ–X+1). If not, number of newly crystallized capsules is equal to (Δn_τ–X). This approach gains importance when number of capsules or time step in the analysis is small.

Number of capsules that have begun freezing becomes $n(\mathrm{t}) = \sum_{\tau<t} \Delta n_{\tau}$ and number of uncrystallized capsules is $n_{unc}(t) = N - n(t)$

State of a single capsule is determined by below statement.

completely - liquid	if $0 = \Delta n$
liquid - solid mixture	if $0 < \Delta n$ & $0 < r_c(t)$
completely - solid	if $r_c(t) \approx 0$

During the cooling of capsules, three states which are mentioned above can be observed at the same time in different capsules due to the stochastic character of freezing. Therefore, total heat exchange between capsules and HTF becomes:

$$\dot{Q}_L(t) = \dot{q}_L(\mathrm{t})\,\mathrm{n}_{unc}(\mathrm{t}) \qquad if\ \ t < \tau$$
$$\dot{Q}_c(t) = \sum_{\tau<t} \Delta n(t)\,\dot{q}_c(t) \qquad if\ \ \tau < t < t_{f,t}$$
$$\dot{Q}_s(t) = \dot{q}_s(\mathrm{t})\,\mathrm{n}_f(\mathrm{t}) \qquad if\ \ t_f < t$$

Total heat transfer from the capsules becomes:

$$\dot{Q}(t) = \dot{Q}_L(t) + \dot{Q}_c(t) + \dot{Q}_s(t) \tag{19}$$

Unlike melting, latent and sensible heat transfer may be observed in different groups of capsules at the same time step.

2.1.2. Modeling of the Tank

The tank includes capsules of PCM and maintains a uniform flow over the capsules. Previous studies [37] have proved that vertical alignment gives better results than horizontal because free convection can be eliminated if the flow is in the opposite direction of free convection. In the present study, tank is aligned vertically. Main assumptions are listed below:

- Heat transfer by conduction is negligible.
- Temperature in the tank is independent from r- direction. [38]
- The tank is perfectly insulated.
- Negligible free convection

Tank is equally divided to *P* layers. Capsules in each layer are assumed to be identical in terms of temperature inside capsules, and heat exchange between each capsule and HTF excluding the freezing duration. On the other hand, capsules inside the same group act identically when freezing begins. Schematic of a layer is presented in Figure 11.

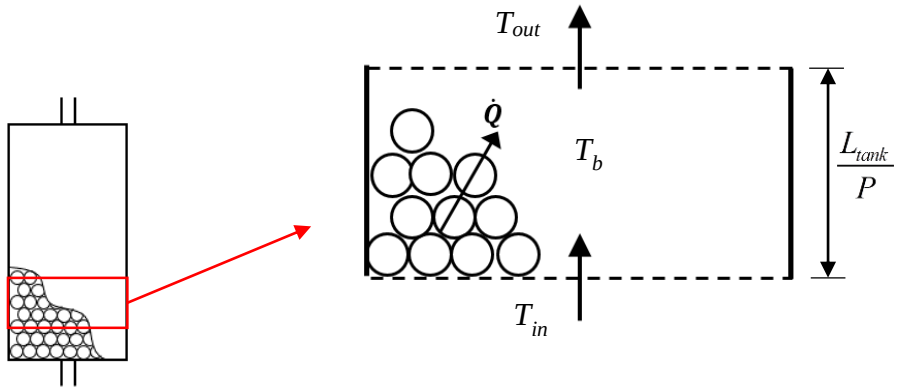

Figure 11. Schematic of a layer in the tank

Energy equation for each layer is given in Equation (20).

$$\rho c V_{lay} \frac{dT_b}{dt} = \rho c \dot{V} \left(T_{in} - T_{out} \right) + \dot{Q}(t) \tag{20}$$

T_b is the average temperature of each layer, $T_b = (T_{in} + T_{out})/2$

T_{in} and T_{out} are the inlet and the outlet temperatures of the layers respectively.

ρ and c are density and specific heat of the HTF.

V_{lay} and $\dot{V}$ are the volume of the layer and volumetric flow rate of the HTF.

2.1.2.1. Pressure Drop through the Tank

Pressure drop in the TES tank may be an important consideration due to its direct influence on storage pressure and turbine power output. One of the main concerns of TES design will be to achieve small pressure drop. Pressure drop in the TES tank is specified as [34]:

$$\Delta p = f \frac{\rho v_s^2 L_{tank}}{D_{eq}} \frac{1-\varepsilon}{\varepsilon^2} \tag{21}$$

where f is the friction factor and calculated using Reynolds number found in Equation (7).

$$f = \frac{150}{\mathrm{Re}} + 1.75 \tag{22}$$

2.2. Validation of LHTES Model

In order to validate that mathematical model gives accurate results, an experimental study is considered and the same conditions with experiment is implemented in the model. The experimental study of Bedecarrats *et al.* [39] is considered for the verification of the model. Authors of this study conducted some other studies about LHTES ([33], [37], [38]) and Bedecarrats [35] conducted a study on mathematical modeling of supercooling phenomenon.

In this study [39], experimental study is based on the cool thermal energy storage containing water as PCM. Schematic of the TES tank is presented in Figure 12.

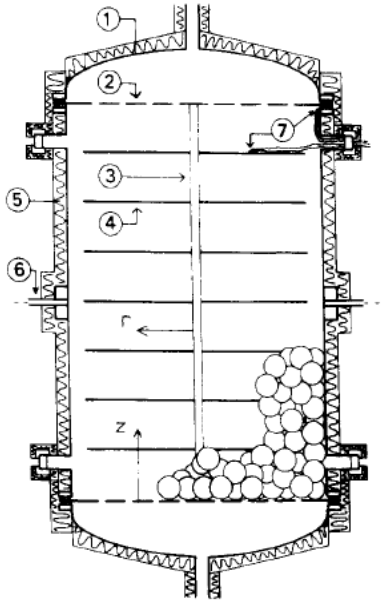

Figure 12. Schematic of the TES tank used in the experiment (Retrieved from [39]).

In the experiment, about 140 thermocouples were located at different locations in the tank and on the surfaces of capsules. Crystallization time can be detected with these measurements. The test setup provide the working fluid at a variety of temperatures. Flow rate can also be controlled. The by-pass allows changing flow direction in the tank for effectively cooling and heating the capsules.

In order to verify the accuracy of the present model, the same operating conditions in the experiment are implemented into the mathematical model. Bedecarrats *et al.* [39] used water as PCM in polyethylene envelope. HTF is monoethylene glycol. Operating conditions in the experiment are presented in Table 3. In Table 4, thermodynamic properties of water and monoethylene glycol can be found.

Table 3. Parameters used in the experiment

Parameter	Abbreviation	Value	Unit
Outer radius of the envelope	r_o	0.0385	m
Inner radius of the envelope	r_i	0.0365	m
Number of capsules in the tank	N	2500	-
Total volume of the tank	V_{tank}	1	m^3
Heat transfer coefficient	h	130	$Wm^{-2}K$
Volumetric flow rate of HTF	$\dot{V}$	1.3 (cooling) 1.1 (heating)	m^3h^{-1}

Table 4. Thermodynamic properties of liquid water, ice and monoethylene glycol [35]

Density			
Liquid Water	ρ_L	1000	$kg\ m^{-3}$
Ice	ρ_s	917	$kg\ m^{-3}$
Monoethylene Glycol	ρ	1082	$kg\ m^{-3}$
Specific Heat			
Liquid Water	c_L	4.22	$kJ\ kg^{-1}K^{-1}$
Ice	c_s	2.04	$kJ\ kg^{-1}K^{-1}$
Monoethylene Glycol	c	3300	$kJ\ kg^{-1}K^{-1}$
Conductivity			
Liquid Water	k_{eq}*	1.1	$W\ m^{-1}K^{-1}$
Ice	k_s	2.25	$W\ m^{-1}K^{-1}$
Monoethylene Glycol	k	0.42	$W\ m^{-1}K^{-1}$
Latent Heat of Fusion			
Water	L_F	333	$kJ\ kg^{-1}$

*Liquid density is higher than solid density. Existence of porosity during melting is compensated with an equivalent conductivity [33]

Boundary and initial conditions for both experimental and mathematical analyses are presented in Table 5.

Table 5. Boundary and initial conditions

	MODE	
	Cooling	Heating
Initial Temperature of the Tank Inlet and Tank (^{0}C)	5.9	-5.5
Final Temperature of the Tank Inlet (^{0}C)	-5.9	5.5
Cooling/Heating Rate (^{0}C/h)	3.5	11
Number of Layers	4	4
Time Step	60	5

Heat transfer coefficient is found as 126 W m^{-2} K^{-1} based on Equation (6) with C=1 [33] which is very close to experimental value (130 W m^{-2} K^{-1}) [39]. However, this value is used only during phase change. During PCM is completely solid or liquid, effective heat transfer coefficient is used, which is 107 W m^{-2} K^{-1} if PCM is liquid, 88 W m^{-2} K^{-1} if PCM is solid inside capsules.

2.2.1. Results of the Present Model

With the conditions specified in Table 3, temperature distribution inside LHTES tank is presented in Figure 13 and Figure 14 during cooling and heating respectively.

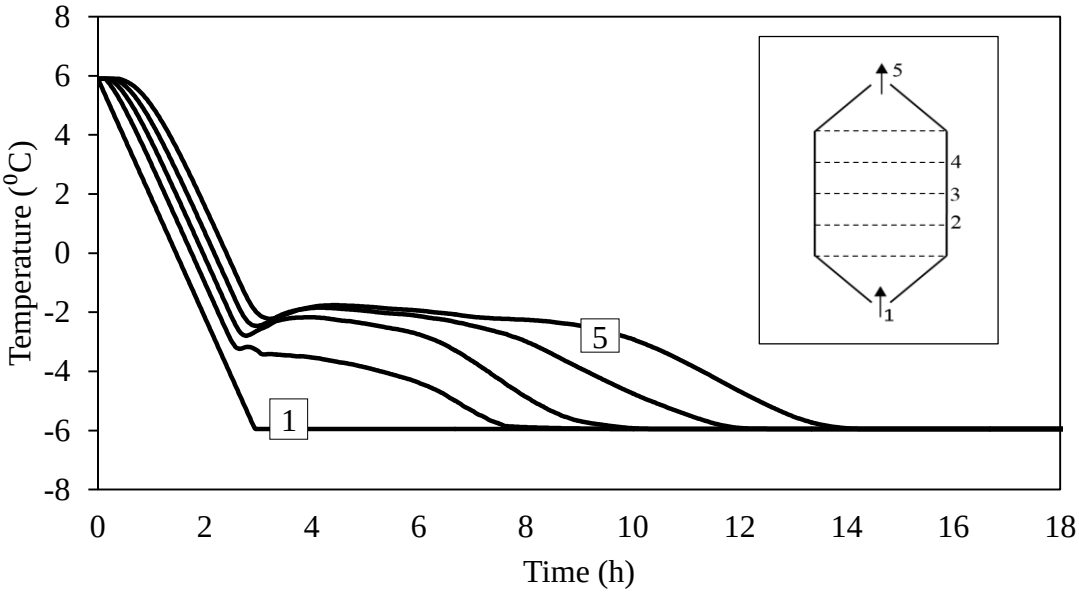

Figure 13. Temperature distribution of HTF in the LHTES tank during cooling for the operating conditions specified in Table 3.

HTF starts to cool down from 5.9 °C until melting point. Due to supercooling and stochastic nature of freezing, PCM temperature does not stabilize at melting point, 0 °C but decreases to minus temperatures. Therefore air temperature also decreases to minus temperatures without stabilization. Stabilization temperature is about -2 °C.

In Figure 14, the process is reversed. Initial temperature of HTF and PCMs is -5.5 °C and process continues until system reaches to 5.5 °C. Temperature distribution inside LHTES is presented in Figure 14.

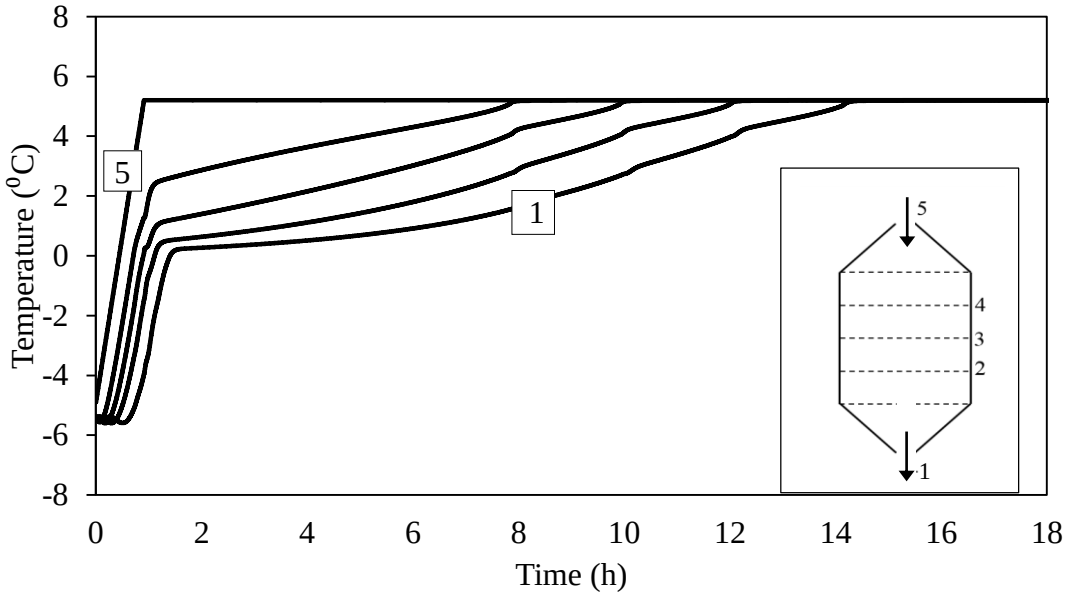

Figure 14. Temperature distribution of HTF in the LHTES tank during heating for the operating conditions specified in Table 3.

During heating the tank, PCMs start to melt at exactly melting point, 0 °C therefore HTF temperature stabilizes at 0 °C then reaches to final temperature.

2.2.2. Comparison of the Results of Experiments and Mathematical Model

In this section, results of the present study are compared with the experimental results. Figure 15 and Figure 16 show the comparison for cooling and heating mode respectively.

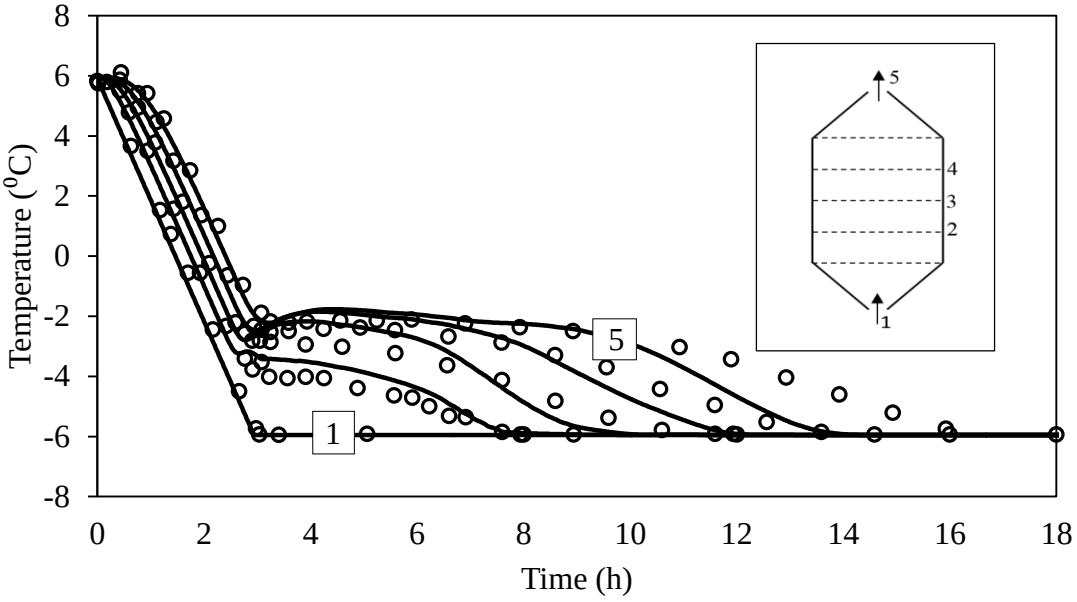

Figure 15. Temperature distribution of HTF in the LHTES tank during cooling compared with the experimental results

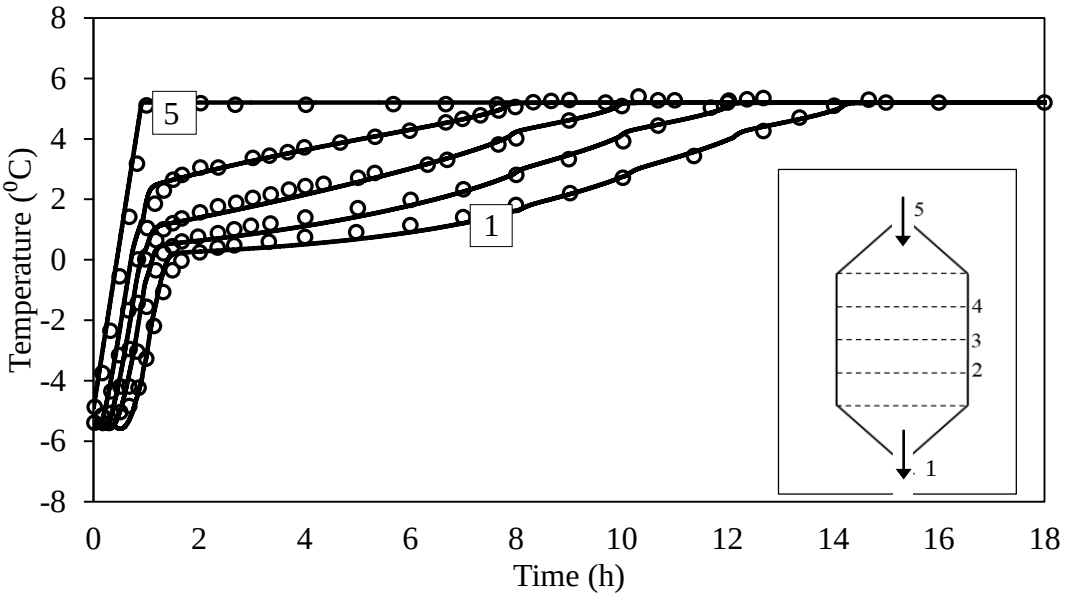

Figure 16. Temperature distribution of HTF in the LHTES tank during heating compared with the experimental results

The model and the experimental results are in a good agreement as can be seen in Figure 15 and Figure 16. Figure 15 shows more discrepancy due to randomization of freezing. In Figure 15, process duration is not well predicted and after the second layer, temperature profiles are not perfectly fitted while it is fitted in Figure 16. Freezing is not perfectly predicted. Figure 16 indicates that if exact time when freezing starts can be predicted, model results will be more coherent.

The present model assumes that tank is perfectly insulated; however, perfect insulation cannot be achievable. For both freezing and melting stages, only latent heat is assumed to be stored. However, sensible heat is also stored in the liquid layer during melting and solid layer during freezing. Furthermore, due to the explicit scheme, there are small oscillations at the beginning of the storage which can be eliminated by implicit scheme but implicit scheme results in a set of nonlinear equations which requires a higher computation effort.

Despite the discrepancies, model gives accurate results and can be adapted to further analyses regarding CAES.

2.3. Parametric Study for Sizing Thermal Energy Storage

In this section, performance of different storage materials inside different sizes of tank and capsules are investigated. In this section, HTF is air corresponding to CAES systems. For sizing, melting process is taken into account considering compression part of CAES. After effective TES size is determined for compression stage, the TES can be analyzed under different mass flow rates in expansion stage.

Mass flow rate of air, boundary and initial conditions of the problem are fixed and presented in Table 6. In Table 7, air properties used in the analysis are presented.

Table 6.Initial and boundary conditions of the analysis

Mass flow rate of air	20	kg/s
Initial Temperature of TES (Air and PCM)	300	K
Temperature of Incoming Air	450	K

Table 7. Air properties at 300 K [31]

Density	ρ	1.1614	kg/m^3
Constant pressure specific heat	c_p	1007	J/kg-K
Thermal conductivity	k	0.0263	W/m-K
Kinematic viscosity	ν	0.00001589	m^2/s
Prandtl number	Pr	0.707	-

There is a large number of substances which are capable of being used as PCM with a wide range of melting temperatures [18]. For the present study, two different PCMs from different classes are selected: paraffin wax (organic) and $MgCl_2 \cdot 6H_2O$ (inorganic-salt hydrate). For comparison, rock is also selected as sensible heat storage material. Properties of these materials are presented in Table 8.

Table 8. Properties of PCMs used in the analyses[18],[40],[41],[42].

	M. P. (K)	**Heat of Fusion (kJ/kg)**	**Density (kg/m^3)**		**Specific Heat (kJ/kg-K)**		**Thermal Conductivity (W/m-K)**	
Name			**L**	**S**	**L**	**S**	**L**	**S**
$MgCl_2 \cdot 6H_2O$	390	168.6	1450	1570	2.6	2.25	0.57	0.71
Paraffin wax	337	173.6	790	916	2.5	2.9	0.17	0.35
Rock	-	-	-	2240	-	1.0	-	2.5

In addition to different materials, parametric study is conducted in order to investigate the effects of tank and capsule sizes on stored heat, storage duration and pressure drop. For tank length of 10 m, cross sectional area, A_{tank} = 10, 20, 30, 40, 50 m and radius of capsules, r_o= 0.04, 0.07, 0.1 m are implemented and results associated with these parameters are presented in the following sections.

2.3.1. Heat Storage

Heat storage should be maximized for an effective heat storage. Amount of stored heat depends on tank volume linearly because the porosity of the tank is kept constant so mass is fixed. For the same type of PCM in the same volume, stored heat is the same. In Figure 17, the change in stored heat is presented for different materials and different volumes.

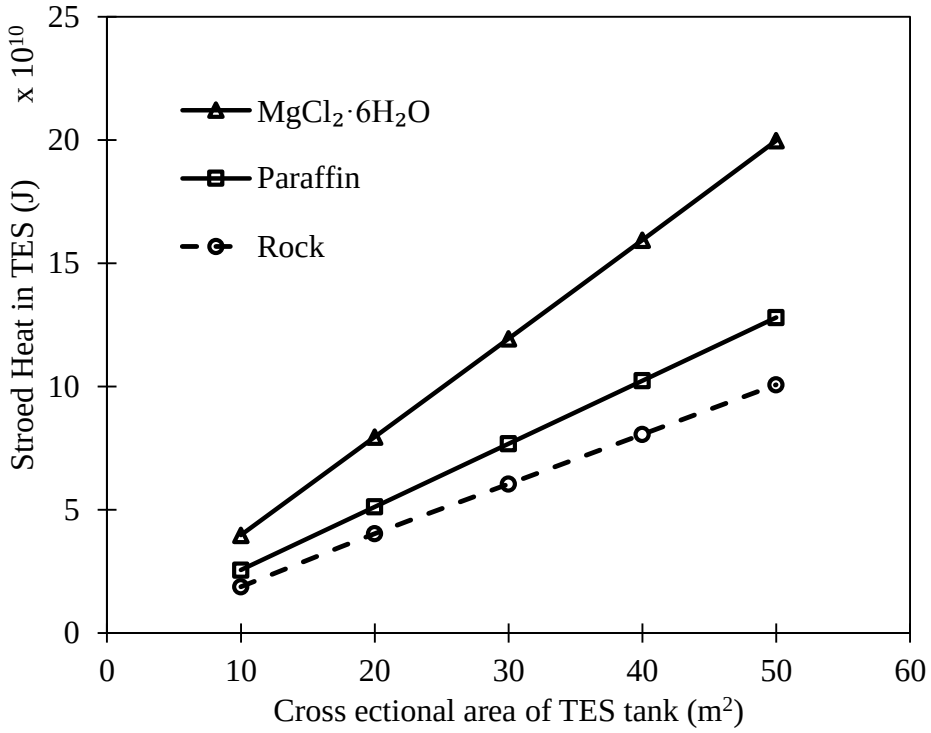

Figure 17. Stored heat versus cross-sectional area of the tank for three different materials. (L_{tank}=10 m)

In Figure 17, an interesting result is presented that although latent heat of paraffin is more than latent heat of magnesium chloride hydrate ($MgCl_2 \cdot 6H_2O$), amounts of stored heat are not in that manner. The reason for this result is density. Because density

of $MgCl_2 \cdot 6H_2O$ is almost double of paraffin's, it can store more heat in the same volume. If same mass is considered instead of volume, paraffin might be a better choice.

As expected, rock provides the poorest performance compared to other materials. For the same storage capacity, even two times larger tank compared to $MgCl_2 \cdot 6H_2O$ is necessary for rock. This fact is due to two reasons. First, rock has a lower volumetric heat capacity (ρc) than $MgCl_2 \cdot 6H_2O$ therefore $MgCl_2 \cdot 6H_2O$ would be a better choice for the same tank dimensions even as a sensible heat storage material. Second, although rock and paraffin have close volumetric heat capacity values, paraffin also experiences phase change and amount of stored latent heat is almost half of the stored heat of rock only during phase change. Consequently, LHTES systems are preferable because of their high heat storage in a same volume and compared to sensible storage. Table 9 summarizes the current discussion quantitatively.

Table 9. Relative amounts of sensible and latent heat storage in a 20 m^2 - 10 m tank filled with different heat storage materials (GJ)

Material	Q_{sen}	Q_{lat}	Q_{tot}	Q_{lat}/ Q_{tot} (%)
$MgCl_2 \cdot 6H_2O$	47.84	31.76	79.60	39.9
Paraffin wax	35.85	19.08	54.93	34.7
Rock	40.32	0	40.32	0

Q_{sen}, Q_{lat} and Q_{tot} refer sensible, latent and total heat storage.

2.3.2. Charge Duration

Charge duration is the first time when outlet temperature of air reaches to inlet air temperature and should be kept at minimum. In an effective TES design, the largest amount of heat should be stored in a minimum volume and at shortest time. Materials are investigated in terms of heat storage per unit volume in the previous section. In this

section, required storage durations for different heat storage mediums are discussed. Storage time is directly related with the heat transfer rate between storage medium and HTF. If the heat transfer is larger, time rate of TES temperature would be larger in Equation (20).

Heat transfer depends on convective heat transfer coefficient which is related with tank cross sectional area, radius of capsules and material properties. Increase in the cross sectional area results in decrease in superficial velocity of HTF. Therefore Reynolds and Nusselt numbers decreases and heat transfer decreases. As a consequence, storage duration is expected to increase with increase in tank cross sectional area.

As radius of PCM capsules/rock spheres increases, Reynolds number increases. On the other hand, increase in the radius results in a smaller *dr/dt* rate for PCMs according to Equation (11) therefore radius has also a negative effect on storage time.

Effects of cross sectional area of the tank, A_{tank} and outer radius of PCM capsules and rock spheres, $r_{o,}$ are investigated and presented in Table 10.

Table 10. Charge durations for TES tanks filled with $MgCl \cdot 6H_2O$, paraffin and rock for different tank and capsule sizes, in minutes

	Area (m^2)	r_o (m)		
		0.0385	0.07	0.1
$MgCl \cdot 6H_2O$	10	304	497	702
	20	507	755	1028
	30	693	992	1306
	40	874	1220	1567
	50	1058	1442	1655
Paraffin	10	137	262	439
	20	213	364	544
	30	286	452	653
	40	358	535	753
	50	426	617	846
Rock	10	221	291	362
	20	405	509	613
	30	583	715	845
	40	758	914	1067
	50	931	1108	1283

Table 10 shows the variation of the storage duration with cross sectional area of tank and radius of capsules. As expected, storage duration increases with increasing tank area and capsule size. On the other hand, different materials show different behavior for change in tank dimensions and capsule radius in terms of storage duration.

Different than rock, phase change period is a consideration for PCMs. Phase change duration is affected by material properties. One parameter that affect the storage duration may be the melting temperature. At the beginning of the process, air and PCM are at close temperatures up to melting point. After PCM reaches the melting point, it remains at constant melting point and air temperature increases by heat transfer from PCM capsules. Heat transfer rate increases with the increasing temperature difference. Therefore, since melting point of paraffin (337 K) is closer to the initial temperature (300 K) than that of $MgCl_2.6H_2O$, process takes shorter time for paraffin. Another

parameter may be the volumetric latent heat (ρL_F) of PCMs. Even if heat transfer rate is the same, volumetric latent heat of $MgCl_2.6H_2O$ (244.5 MJ/m^3) is larger than paraffin's (137.1 MJ/m^3) then change in radius become smaller according to Equation (11).

For rock, storage duration does not vary with radius significantly. Effect of material radius on PCMs is more critical than that on rock.

To decrease storage duration, capsules with small radius should be selected. Cross sectional area of tank, additionally, should be kept small to keep storage duration minimum. For the storage mediums, paraffin provides a shorter storage duration than other substances which make paraffin competitive with $MgCl_2.6H_2O$.

2.3.3. Metric for Determination of the Proper PCM and Dimensions

For TES systems, maximum heat is desired to be stored in shortest time. For this purpose, a performance metric which is amount of stored heat per unit time (SHPUT) is generated in order to select the most proper design.

With the data obtained in Sections 2.3.1 and 2.3.2, different SHPUT values for different materials, and tank and capsule sizes are presented in Table 11.

Table 11. Change in SHPUT with change in tank cross sectional area (A_{tank}) and capsule radius (r_o) (10^8 J / min)

	Area (m^2)	r_o (m)		
		0.0385	0.07	0.1
$MgCl \cdot 6H_2O$	10	1.80	1.18	0.84
	20	1.98	1.49	1.14
	30	2.10	1.66	1.31
	40	2.20	1.78	1.43
	50	2.27	1.87	1.53
Paraffin	10	2.66	1.47	0.91
	20	3.39	2.09	1.42
	30	3.85	2.46	1.77
	40	4.25	2.71	2.01
	50	4.65	2.90	2.22
Rock	10	0.77	0.61	0.60
	20	0.86	0.70	0.69
	30	0.90	0.75	0.74
	40	0.93	0.66	0.68
	50	0.95	0.81	0.80

According to Table 11, paraffin provides the best heat storage per unit time. $MgCl_2 \cdot 6H_2O$ is not better than paraffin despite superior heat storage capacity among others. Best SHPUT of $MgCl_2 \cdot 6H_2O$ (2.27 10^8 J/min) is about half of the best SHPUT of paraffin (4.6510^8 J/min). Rock has the lowest values of SHPUT which is expected.

2.3.4. Discharge Duration

Effects of different storage materials, size of tank and size of capsules on stored heat and storage duration are analyzed in the previous sections. In this section, effect of mass flow rate of air on discharge duration will be discussed.

In this study, for the application of TES to CAES, during charging, mass flow rate of air is assumed to be specified by compressor, which will be discussed in Chapter 3 in detail. However, for the discharge period, air mass flow rate may be adjusted to meet desirable conditions.

For the analysis, a representative condition is considered for $MgCl_2 \cdot 6H_2O$ and paraffin. Cross-sectional area and length of the tank is 30 m^2 and 10 m. Storage duration for $MgCl_2 \cdot 6H_2O$ in the same tank dimensions is 660 minutes and that is 286 minutes for paraffin. In Table 12 and Table 13 for specified mass flow rates are presented.

Table 12. Storage and discharge durations of $MgCl_2 \cdot 6H_2O$ in 30 m^2 – 10 m tank.

$\dot{m}_{air}$ (kg/s)	**Storage Duration (min)**
20	660
	Discharge Duration (min)
20	1006
40	611
50	522

Table 13. Storage and discharge durations of paraffin in 30 m^2 – 10 m tank.

$\dot{m}_{air}$ (kg/s)	**Storage Duration (min)**
20	286
	Discharge Duration (min)
20	1003
40	607
60	459
80	398
100	348
150	321
200	289
250	223

According to the results, same amount of heat stored during charging can not be recovered in discharging period with the same mass flow rate. About a two times greater mass flow rate is required to achieve the same heat recovery or process takes two times longer. The reason why discharge duration is about two times longer than storage duration with the same flow rate is the stochastic nature of freezing. Because

capsules start to freeze at different times, capsules remain at around melting temperature for longer. Therefore for discharge period, selecting a higher mass flow rate is required.

Furthermore, this analysis strengthens the relationship between melting temperature and storage duration. Melting point of $MgCl_2 \cdot 6H_2O$ is at about middle of the temperature limits and discharge takes two times longer than charge. On the other hand, melting point of paraffin is closer to the lower temperature limit and discharge takes about five times longer than charge with the same mass flow rate. Stochastic nature of freezing can explain the delay but the difference of discharge durations between two materials may be explained by melting points. It may be desirable to select a PCM, of which melting point is at the middle of the temperature limits of the application.

Discharge duration for rock is calculated as 540 minutes. Charge duration for rock was 580 minutes and this finding may be a clue for that supercooling and stochastic nature of freezing result in longer discharge durations than charge durations for PCMs.

2.3.5. Heat Transfer Coefficient

Convective heat transfer is determined using dimensionless Nusselt number. Equation (6) provides information about heat transfer coefficient. Heat transfer coefficient is affected by HTF type and tank geometry and capsule size. On the other hand, as discussed in Section2.1.1, Biot number is checked for validity of lumped capacitance assumption and heat transfer coefficient is corrected if Biot number is greater than 0.1 according to Equation (2). In this section, corresponding heat transfer coefficients of the parametric study are presented. First, Biot numbers of the applications of different materials, tank and capsule sizes are presented in Table 14. For ease of presentation, Biot numbers for smaller thermal conductivity of liquid or solid are presented.

Table 14. Biot number for different tank dimensions and capsule sizes

	Area (m^2)	Capsule Radius (m)		
		0.0385	0.07	0.1
$MgCl_2 \cdot 6H_2O$	10	1.47	1.98	2.37
	20	1.04	1.40	1.68
	30	0.85	1.15	1.37
	40	0.74	0.99	1.19
	50	0.66	0.89	1.06
Paraffin	10	2.99	4.04	4.83
	20	2.12	2.85	3.41
	30	1.73	2.33	2.79
	40	1.50	2.02	2.41
	50	1.34	1.81	2.16
Rock	10	0.41	0.56	0.67
	20	0.29	0.40	0.47
	30	0.24	0.32	0.39
	40	0.21	0.28	0.33
	50	0.19	0.25	0.30

According to the results in Table 14, Biot number is greater than 0.1 for all cases. Therefore correction is required to obtain more accurate results. In Table 15, effective heat transfer coefficients are presented.

Table 15. Effective heat transfer coefficients corrected based upon Equation (2).

Effective Heat Transfer Coefficient, h_{eff} ($Wm^{-2}K^{-1}$)				
	Area (m^2)	Capsule Radius (m)		
		0.0385	0.07	0.1
$MgClH_2O$	10	42.87	27.33	20.67
	20	35.14	22.98	17.65
	30	30.87	20.48	15.88
	40	28.00	18.76	14.63
	50	25.88	17.47	13.69
Paraffin	10	28.87	17.49	12.86
	20	25.14	15.60	11.62
	30	22.88	14.41	10.82
	40	21.26	13.54	10.23
	50	20.02	12.85	9.76
Rock	10	64.65	44.84	35.76
	20	48.55	34.22	27.60
	30	40.76	28.96	23.49
	40	35.90	25.64	20.86
	50	32.49	23.28	19.00

Original heat transfer coefficients were presented in Table 16. Heat transfer coefficients are found using Reynolds and Prandtl numbers therefore they are independent of material properties.

Table 16. Heat transfer coefficients for the parametric study based upon Equation (6)

Heat Transfer Coefficient, h ($W\ m^{-2}\ K$)			
Area (m^2)	Capsule Radius (m)		
	0.0385	0.07	0.1
10	80.72	59.87	50.09
20	57.08	42.33	35.42
30	46.61	34.56	28.92
40	40.36	29.93	25.04
50	36.10	26.77	22.40

Effective heat transfer coefficient approach is reasonable. Lumped capacitance assumption overestimates heat transfer because there is actually temperature variation inside PCM capsules or rock spheres. Effective heat transfer coefficient decreases heat transfer rate in order to compensate the temperature variation inside capsules.

2.3.6. Pressure Drop

Pressure drop is independent of PCM type but only depends on tank and capsule sizes. As Equation (21) indicates, pressure drop depends on PCM capsule radius, cross section area and length of tank. In this section, effects of these parameters are investigated.

In Figure 18, effects of cross sectional area, A_{tank}, and length, L_{tank}, of the tank on the pressure drop can be observed. Length has a linear effect on pressure drop with a constant slope for fixed A_{tank} and r_o, which is an expected result.

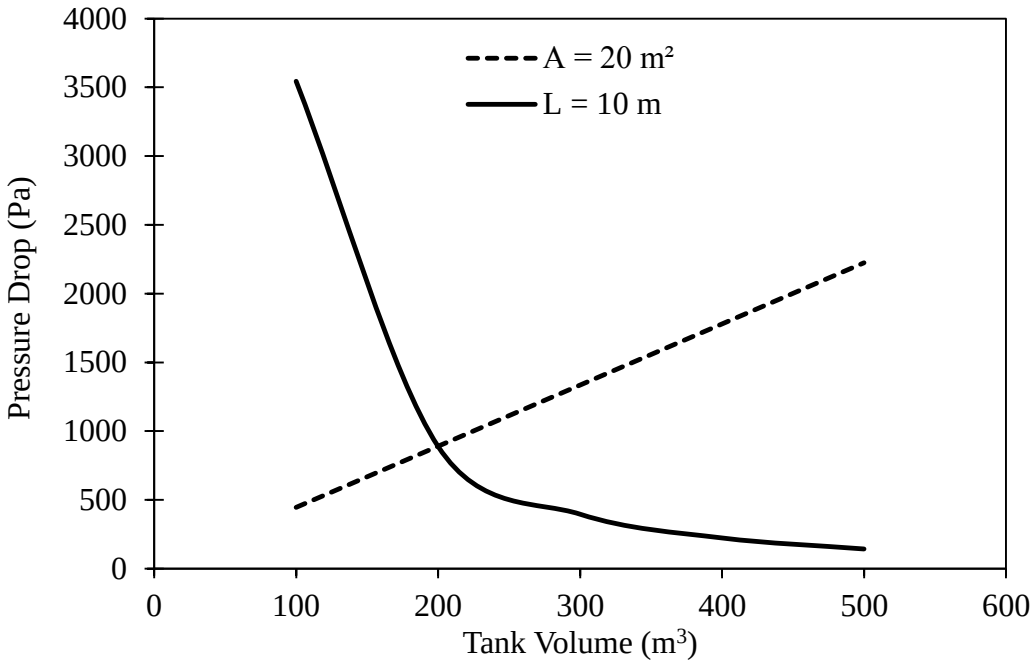

Figure 18. Pressure drop through the tank with different tank volumes (r_o = 0.05 m)

Radius has a similar effect on pressure drop like cross sectional area of tank as can be seen in Figure 19. Figure 19 also shows that change in the pressure drop is smaller as capsule size increases. Furthermore, pressure drop is observed to be much higher in large A_{tank}, smaller r_o data sets.

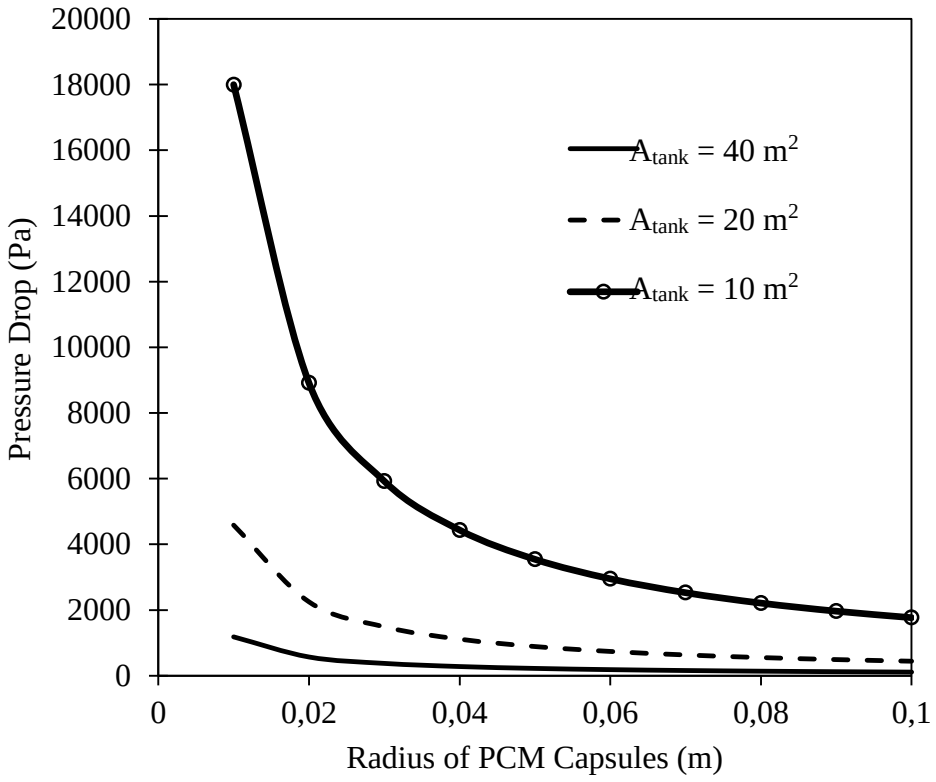

Figure 19. Pressure drop through the tank with different capsule sizes in different tank volumes (L_{tank} = 10 m)

For the design of TES, cross sectional area of the tank and PCM capsules should be as large as possible and shorter tanks should be preferred regarding pressure drop by contrast with storage duration concern which is discussed in Section 2.3.2. Consequently, TES sizing is the optimization of tank and capsule dimensions considering desired amount of stored heat, duration of storage and pressure drop.

2.4. Conclusion

In this chapter, mathematical modeling of LHTES is presented. The present model can be modified as setting latent heat zero to be used to model SHTES.

Model is validated with experimental data and used for different parametric studies. In the parametric studies, there are several significant results.

The most important result in this chapter is that PCMs are seem to be better than sensible heat storage material, rock in terms of heat storage per volume and per storage duration. In Chapter 3, comparison of latent and sensible thermal storage systems will be based on CAES performance.

PCMs provide good storage properties such as high stored energy and comparable storage durations. On the other hand, there are several drawbacks related with the PCMs. First, incompatible charging and discharging durations may be problematic when LHTES is used in CAES. Second, supercooling may be a problem for salt-hydrates. In this study, supercooling characteristics of water are assumed as valid for the other materials but $MgCl_2 \cdot 6H_2O$ should be investigated in terms of supercooling. Although paraffin can not store heat as much as $MgCl_2 \cdot 6H_2O$, it has certain advantages considering storage duration. However, discharge takes more time for paraffin.

Pressure drop is calculated for CAES and it may be an important consideration for CAES since decrease in pressure results in loss of performance.

In Chapter 3, thermodynamic modeling of CAES is presented and a case study is considered to observe the operation of CAES in a simple operating condition with different TES systems.

CHAPTER 3

COMPRESSED AIR ENERGY STORAGE MODEL WITH THERMAL ENERGY STORAGE

3.1. Introduction

In this chapter, the other components of CAES system are presented. Present CAES system comprises compression and expansion stages, thermal energy storage (TES) and air storage. Theoretical background and sizing methodology of a TES system is discussed in Chapter 2. In this Chapter, remaining components of CAES will be modeled and effects of different parameters and different TES designs on CAES performance will be accounted. In Figure 20, a simple sketch of the single stage compression and expansion system is presented. Ambient air (state a) is compressed to a high pressure (state b). Before storing compressed air in the storage, thermal energy of compressed air is stored in TES. While discharging, pressurized air is drawn from air storage and heated with the stored heat in TES and expanded from state *e* to *f* in the turbine.

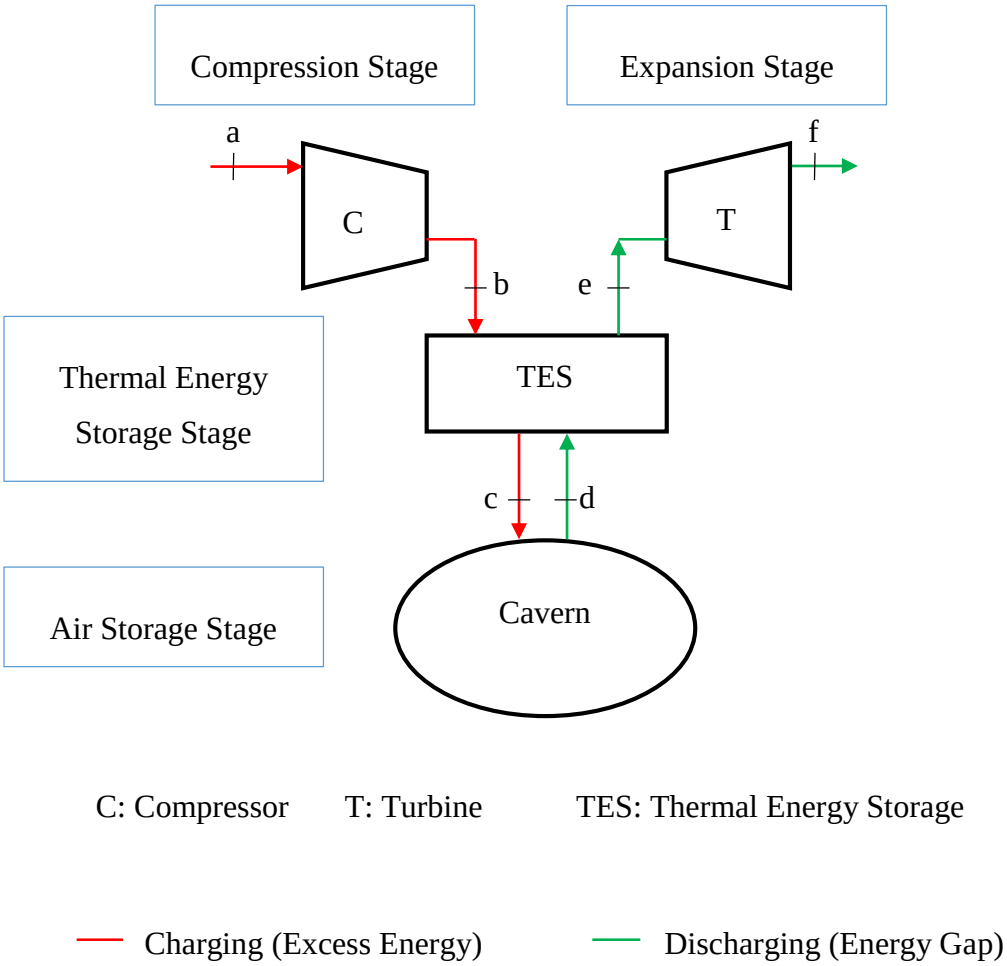

Figure 20. Sketch of CAES system with TES

3.2. Mathematical Model

In this section, compression stage, air storage and expansion stage are modeled. Process is transient like TES model however only thermodynamic models for compressor, turbine and compressor are included but detailed analyses are not included in the present study.

During compression, air at ambient temperature and pressure is compressed and sent to TES. Pressure drop in TES is discussed in Section 2.3.6. Constant volume air storage is filled with air which is pressurized by compressor and cooled by TES until pressure of air inside cavern reaches to the specified maximum allowed pressure. Air is assumed at ambient temperature inside air storage and heat is assumed to be lost to the surroundings at the moments when air first enters to the storage and is being drawn from the storage. There is no thermal interaction between air and surroundings during storage. During discharge, air is heated with the thermal energy which is stored during compression.

3.2.1. Compression Stage

In this section, theory of a single stage compression process will be presented. The assumptions which are made in the model of compression stage are listed below.

- Each compressor is modeled as adiabatic with an isentropic efficiency of 0.9.
- Compression process is polytropic.
- Initial start-up duration is neglected.
- Air is an ideal gas.
- Constant specific heats

1st Law of Thermodynamics is applied to the compressor:

$$\dot{W}_c = \dot{m}_{air,c}\left(h_a - h_b\right) \tag{23}$$

where $\dot{m}_{air,c}$ is the mass flow rate through the compressor, h is enthalpy, states a and b compressor inlet and exit respectively. Isentropic efficiency for a compressor is defined as $\eta_c = \frac{\dot{W}_{c,rev}}{\dot{W}_c}$ and reversible compressor power is determined as

$$\dot{W}_{c,rev} = \dot{m}_{air,c}\left(h_a - h_b^s\right) \tag{24}$$

where superscript "s" refers to isentropic. Equation (23) may be restated using the definition of isentropic efficiency and Equation (24).

$$\dot{W}_c = \frac{1}{\eta_c}\dot{m}_{air,c}\left(h_a - h_b^s\right) \tag{25}$$

Air is an ideal gas and enthalpy of air can be found as $h - h_{ref} = c_p\left(T - T_{ref}\right)$ relative to a reference. Equations (23), (24) and (25) becomes:

$$\dot{W}_c = \dot{m}_{air,c}c_p\left(T_a - T_b\right) \tag{26}$$

$$\dot{W}_{c,rev} = \dot{m}_{air,c}c_p\left(T_a - T_b^s\right) \tag{27}$$

$$\dot{W}_c = \frac{1}{\eta_c}\dot{m}_{air,c}c_p\left(T_a - T_b^s\right) \tag{28}$$

Actual air temperature at the exit of compressor can be determined by equating Equations (23) and (25).

$$T_b = T_a - \frac{1}{\eta_c}\left(T_a - T_b^s\right) \tag{29}$$

Entropies of state "a" and state "b^s" are the same therefore T_b^s can be found from the equality of entropy as in Equation (30).

$$s_2 - s_1 = c_p \ln\left(\frac{T_2}{T_1}\right) - R\ln\left(r_p\right) = 0 \tag{30}$$

r_p is pressure ratio of compressor. Equation (30) reduces to $\left(\frac{T_2}{T_1}\right) = \left(r_p\right)^{\frac{R}{c_p}}$. Considering $c_p - c_v$ = R and c_p / c_v being k, which is specific heat ratio. Therefore T_b^s can be found as

$$T_b^s = T_a \left(r_p\right)^{\frac{k-1}{k}} \tag{31}$$

And Equation (29) can be rewritten as to find actual compressor exit temperature, T_b.

$$T_b = T_a - \frac{1}{\eta_c}\left(T_a - T_a\left(r_p\right)^{\frac{k-1}{k}}\right) = T_a\left[1 - \frac{1}{\eta_c}\left(1 - \left(r_p\right)^{\frac{k-1}{k}}\right)\right] \tag{32}$$

Inlet temperature and pressure, compressor power and pressure ratio are fixed in the compressor model. Actual exit temperature of compressor is found in Equation (32). Mass flow rate can also be found from 1st Law of Thermodynamics and stated in Equation (33).

$$\dot{m}_{air,c} = \frac{\eta_c \dot{W}_c}{c_p T_a\left(1 - \left(r_p\right)^{\frac{n-1}{n}}\right)} \tag{33}$$

Air at the compressor exhaust enters TES with the mass flow rate and at the temperature determined in this section. After thermal energy of air stored in the TES,

air sent to air storage. In the Section 3.2.2, air storage is modeled regarding both charging and discharging and in Section 3.2.3, expansion stage of CAES is discussed.

3.2.2. Air Storage Cavern

Zhang *et al.* [24] proposed different approaches for thermodynamic model of air storage. These models can be listed as

- Constant-volume and constant-temperature model (VT model)
- Constant-volume and adiabatic model (VA model)
- Constant-pressure and constant-temperature model (PT model)
- Constant-pressure and adiabatic model (PA model)

Constant pressure models are appropriate if air is stored by means of underwater bags [43] around which pressure is maintained constant by nature. For the underground caverns or other rigid storage tanks, V-models would be more meaningful. Considering the cavern geographies and industrial tanks, adiabatic approach is not realistic because there will be a temperature difference between TES outlet (storage inlet) and surroundings (cavern structure or ambient). Therefore, VT model is used for the storage model. Throughout the process, air temperature in the storage is assumed to be at ambient temperature.

3.2.2.1. Charging Process

Charging of the storage is modeled as a rigid tank with one inlet. Simple schematic of the storage cavern is presented in Figure 21.

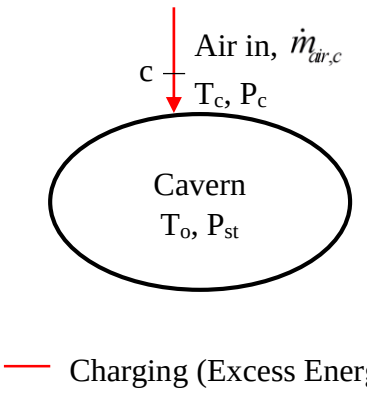

Figure 21. Schematic of air storage during charging

Applying Continuity equation and 1st law of Thermodynamics to the cavern,

$$\frac{dm}{dt} = \dot{m}_{in} \tag{34}$$

$$\frac{d(mu)}{dt} = h_{in}\dot{m}_{in} + \dot{Q} \tag{35}$$

where $\dot{m}_{in}$ is the mass flow rate of air flowing into cavern and equals to $\dot{m}_{air,c}$ and h_{in} is the enthalpy of the incoming air to the cavern which refers to air at the state *c*.

Equation (35) can also be expressed as

$$m\frac{du}{dt} + u\frac{dm}{dt} = h_c\dot{m}_{air,c} + \dot{Q}_{loss,c} \tag{36}$$

du/dt term is zero since temperature inside cavern is assumed constant at T_o. Substituting Equation (34) into Equation (36):

$$\dot{Q}_{loss,c} = \dot{m}_{air,c}\left(u_{st} - h_c\right) \tag{37}$$

Enthalpy can be expressed as $h = u + RT$ and Equation (37) may be expressed as

$$\dot{Q}_{loss,c} = \dot{m}_{air,c}\left[u_{st} - \left(u_c + RT_c\right)\right] \tag{38}$$

$$\dot{Q}_{loss,c} = \dot{m}_{air,c}\left[c_v\left(T_o - T_c\right) - RT_c\right] \tag{39}$$

Heat loss from storage changes with time as air temperature at the exit of TES.

Ideal gas equation determines the change of air mass inside cavern.

$$\frac{dm}{dt} = \frac{V_{st}}{\mathrm{R}T_o}\frac{dP_{st}}{dt} \tag{40}$$

Pressure inside storage changes with air mass inside cavern so with mass flow rate of the air flowing through compression process.

$$\frac{dP_{st}}{dt} = \dot{m}_{air,c}\frac{\mathrm{R}T_o}{V_{st}} \tag{41}$$

3.2.2.2. Discharge Process

Discharge of the storage is modeled as a rigid tank with one outlet. Applying Continuity equation and 1st law of Thermodynamics similar to charging process, governing equations for the air storage cavern are obtained. Since the pressure inside air storage decreases, there will be heat gain from surroundings. Schematic of the storage cavern during discharge is presented in Figure 22.

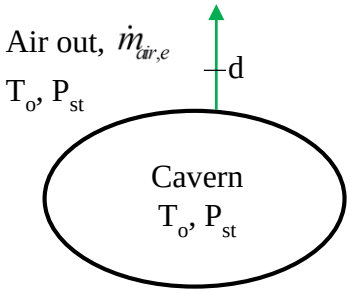

Figure 22.Schematic of air storage cavern during discharging

$$-\frac{dm}{dt} = \dot{m}_{out} \tag{42}$$

$$m\frac{du}{dt} + u\frac{dm}{dt} = -h_{out}\dot{m}_{out} + \dot{Q}_{gain} \tag{43}$$

Like in the charging process, *du/dt* term is zero. $\dot{m}_{out}$ is the mass flow rate through expansion stage, $\dot{m}_{air,e}$. h_{out} refers to the enthalpy of air at state *d*. Heat gain during discharge of cavern is expressed as

$$\dot{Q}_{gain} = \dot{m}_{air,e}\left(h_d - u_{st}\right) \tag{44}$$

If the definition of enthalpy, $h=u+Pv$, is substituted into Equation (44), heat gain becomes:

$$\dot{Q}_{gain} = \dot{m}_{air}\left(\left(u_d + P_d v_d\right) - u_{st}\right) \tag{45}$$

Air is stored at T_o and discharged to expansion stage at the same temperature, $T_d = T_o$. Therefore, $u_{st} = u_d$. In addition, according to ideal gas relation, Pv=RT and Equation (45) becomes

$$\dot{Q}_{gain} = \dot{m}_{air,e} \mathrm{R} T_o \tag{46}$$

Equation (46) shows that heat gain only depends on mass flow rate of air at the discharge process unlike charging process.

During discharging, air pressure inside cavern changes according to ideal gas relation.

$$\frac{dP_{st}}{dt} = \dot{m}_{air,\mathrm{e}} \frac{\mathrm{R} T_o}{V_{st}} \tag{47}$$

3.2.3. Expansion Stage

Expansion process is similar to compression but process is reversed. Assumptions made for compression process are valid for expansion. Governing equations for a single stage turbine is presented in this section.

1st Law of Thermodynamics is applied to the turbine:

$$\dot{W}_t = \dot{m}_{air,e} \left(h_e - h_f \right) \tag{48}$$

where states *e* and *f* are turbine inlet and exit.

Isentropic efficiency is defined as $\eta_t = \frac{\dot{W}_t}{\dot{W}_{t,rev}}$ and reversible turbine power output is determined as

$$\dot{W}_{t,rev} = \dot{m}_{air,e}\left(h_e - h_f^s\right) \tag{49}$$

where superscript "s" refers to isentropic. If Equation (48) is restated using the definition of isentropic efficiency and Equation (49):

$$\dot{W}_t = \eta_t \dot{m}_{air,e}\left(h_e - h_f^s\right) \tag{50}$$

Air is an ideal gas and enthalpy of air can be found as $h - h_{ref} = c_p\left(T - T_{ref}\right)$. Equations (48), (49) and (50)become:

$$\dot{W}_t = \dot{m}_{air,e} c_p\left(T_e - T_f\right) \tag{51}$$

$$\dot{W}_{t,rev} = \dot{m}_{air,e} c_p\left(T_e - T_f^s\right) \tag{52}$$

$$\dot{W}_t = \eta_t \dot{m}_{air,e} c_p\left(T_e - T_f{}^s\right) \tag{53}$$

Air temperature at the turbine exit can be determined by equating Equations (51) and (53).

$$T_f = T_e - \eta_t\left(T_e - T_f^s\right) \tag{54}$$

T_e is the outlet temperature of TES. T_f changes with changing T_e.

Unlike compression process, pressure ratio of turbine is not constant due to variable pressure inside cavern. If the pressure ratio was kept constant, air pressure at the turbine exit might be lower than ambient pressure and reverse flow would occur.

Therefore P_f is assumed to be constant at ambient, P_o, pressure ratio of turbine becomes:

$$r_{p,e} = \frac{P_e}{P_f} \tag{55}$$

Similar with the compression stage, equality of entropy may be used to determine the isentropic exit temperature of turbine.

$$T_f^s = T_e \left(r_{p,e} \right)^{-\frac{k-1}{k}} \tag{56}$$

k is specific heat ratio. For the turbine, mass flow rate, expansion ratio and inlet pressure is known. Inlet temperature is specified by TES. Turbine power output and exit temperature are determined in the model.

Pressure ratio of the turbine is found from Equation (55). Air temperature at the exit of the turbine is determined by using Equations (54) and (56).

$$T_f = T_e - \eta_t \left(T_e - T_e \left(r_{p,e} \right)^{-\frac{k-1}{k}} \right) = T_e \left[1 - \eta_t \left(1 - \left(r_{p,e} \right)^{-\frac{k-1}{k}} \right) \right] \tag{57}$$

Exit temperature of turbine changes with exit temperature of TES, T_e and variable pressure ratio during expansion stage.

Turbine power output can be expressed simply by combining Equations (53) and (54).

$$\dot{W}_t = \eta_t \dot{m}_{air,e} c_p T_e \left(1 - \left(r_{p,e} \right)^{-\frac{k-1}{k}} \right) \tag{58}$$

Equation (58) indicates that turbine power output is proportional to mass flow rate of air and turbine inlet temperature and decreases during expansion stage with decreasing air pressure inside cavern.

3.3. Effects of Different Parameters on Performance of CAES

In this section, effects of parameters on the system performance are investigated. First, relation between mass flow rates at the compression and expansion stages and air storage volume is investigated in Section 3.3.1. Then, parameters affecting heat loss during charging are analyzed in Section 3.3.2. Finally, turbine power is analyzed in Section 3.3.3. In the last section of this chapter, a simple case is studied for both $MgCl_2 \cdot 6H2O$ and paraffin.

3.3.1. Relationship between Air Mass Flow Rate and Volume of Air Storage Cavern

During both charging and discharging periods, there is a relationship between mass flow rate and volume of the cavern, which is previously stated in Equations (41) and (47). Both equations represent the same condition except that rate of pressure change is negative or positive. In general, CAES systems have minimum and maximum operation pressure limits and air storage cavern should provide operation between these pressure limits. Cavern volume is determined considering the pressure limits. Equation (41) is integrated to the limits of P_{min} and P_{max} and Equation (59) is obtained.

$$V_{st} = \left(\dot{m}_{air,c}\Delta t_c\right)\frac{\mathrm{R}T_o}{\left(P_{max} - P_{min}\right)} \tag{59}$$

There is a certain relationship between cavern volume, V_{st}, mass flow rate of air during compression stage, $\dot{m}_{air,c}$ and charging duration, Δt_c. Mass flow rate is determined in Equation (33) according to the compressor power input therefore storage duration changes with desired air storage cavern volume.

On the other hand, Equation (59) is also valid for expansion stage. However, air mass flow rate is not specified by the system but can be adjusted. Therefore discharge duration is estimated using Equation (59).

In this study, storage volume is taken as an input. Mass flow rate of the compression stage is specified by compressor and charging and discharging processes take a time indicated by Equation (59).

In Section 2.3.4 discharge duration was found to be about two times longer than charging duration for $MgCl_2 \cdot 6H_2O$ and about ten times longer for paraffin with the same mass flow rate. This is an interesting result which states that complete heat recovery is impossible with the same tank volume. Even if the mass flow rate of discharge process is taken according to the findings in Section 2.3.4, process can not take the same time with charge process due to pressure limits of air storage.

This situation results in both advantage and disadvantage. Advantage is to obtain high temperature at turbine inlet and disadvantage is partially discharged TES.

3.3.2. Effects of Mass Flow Rate at the Compression Stage and Temperature at TES Exit on Heat Loss to Air Storage Cavern Surroundings

Pressurized air is sent to storage cavern after its thermal energy is stored in TES. In Section 3.2.2, heat loss to surroundings is discussed during charging period. Heat is lost when pressurized air is being sent to cavern during charging because air in the cavern is assumed to be at T_o.

Heat loss during charging is affected only by exit temperature of TES assuming mass flow rate is specified.

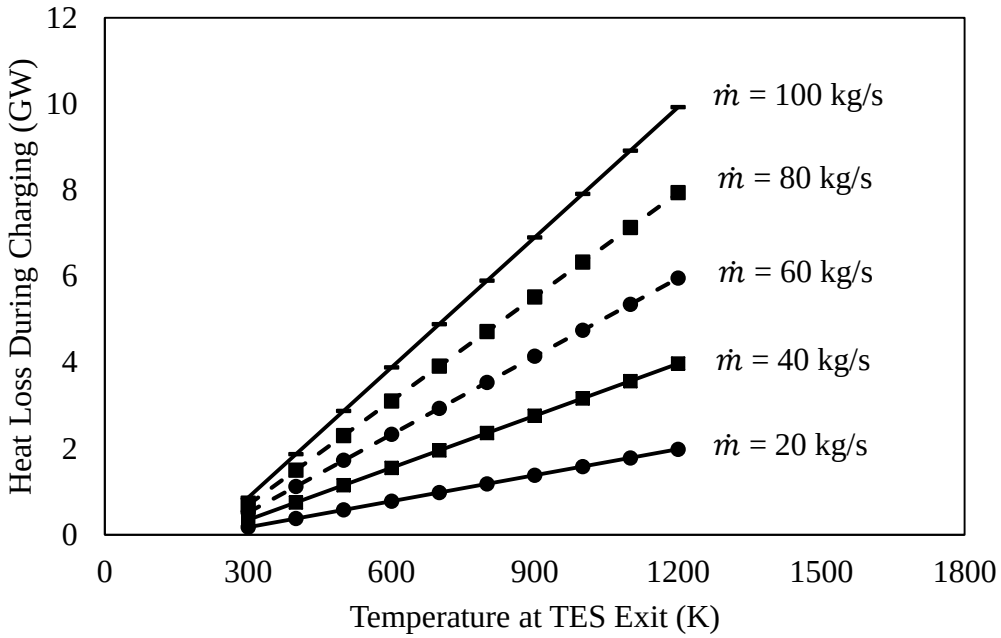

Figure 23. Rate of heat loss during charging with respect to temperature at the TES exit and mass flow rate of air.

According to Figure 23, rate of heat loss to the surroundings increases with increasing mass flow rate and air temperature at TES exit. Because the mass flow rate of air specified by compressor, air temperature at the TES exit should be kept at minimum.

This finding leads to the importance of choice of heat storage medium. An ideal storage medium should have a good heat storage characteristics therefore thermal energy of the air at the compressor exhaust is stored in TES layer by layer. As hot air flows through TES, prior portions of TES should be quickly heated therefore minimum amount of heat is lost in the cavern.

Heat gain during discharge linearly changes with mass flow rate of air at discharge therefore it is not analyzed.

3.3.3. Effect of Exit Temperature of TES and Expansion Ratio of Turbine on Power Output

Power output of the turbine depends on the exit temperature of TES and air pressure in cavern. In order to evaluate this relationship, a hypothetical discharge process is considered in Figure 24. TES is assumed to provide 1000 K air at maximum air pressure in cavern initially. As time passes, thermal energy stored in TES is discharged and exit temperature decreases. Meanwhile, air pressure inside cavern decreases as drawing air from cavern. In Figure 24, x-axes are pressure ratio and TES exit temperature. The hypothetical process is assumed to start with TES exit temperature of 1000 K and pressure ratio of 65 and finished at TES exit temperature of 300 K and pressure ratio of 40.

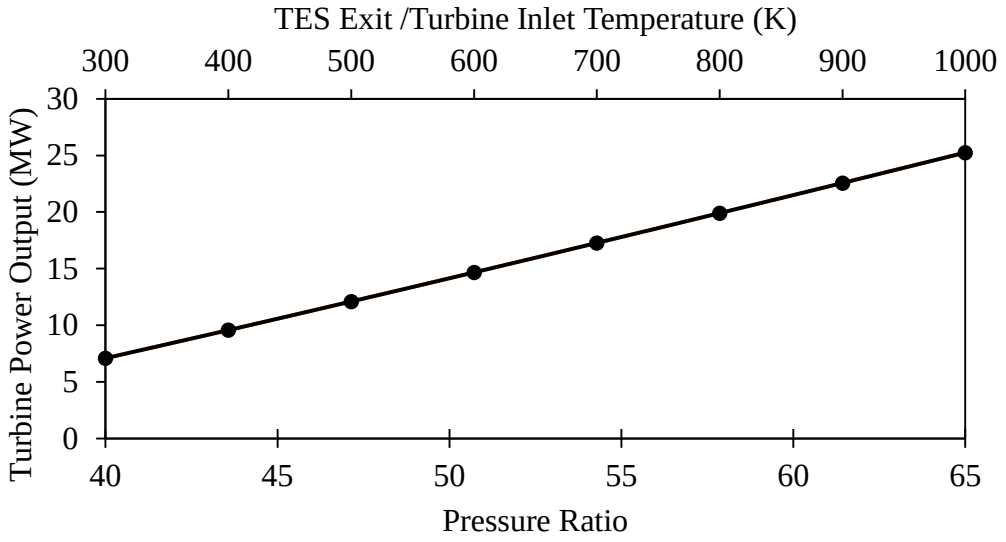

Figure 24. Effects of pressure ratio and exit temperature of TES on turbine power output

Figure 24 shows that turbine power output increases with increasing pressure ratio and temperature at TES exit. This result is expected. In order to increase turbine power output, temperature at TES exit should be kept as higher as possible. In addition,

maintaining higher air pressure in cavern provides longer operation duration and higher turbine work output.

In order to maintain higher pressure in cavern for a longer time, rate of decrease in air storage pressure should be lowered, which is indicated by Equation (47). Rate of decrease in pressure depends on cavern volume. However, larger cavern volume provides longer operation durations also for charging process which may result in partially filled cavern.

Unlike cavern pressure, exit temperature of TES directly affects power output of turbine. Maintaining initial high temperature throughout discharge at TES outlet can be achieved by a proper selection of heat storage medium.

3.4. Case Study: CAES System of 3-Stage Compression and Expansion

In this section, an illustrative case is considered. A three-stage CAES is designed, which is presented in Figure 25.

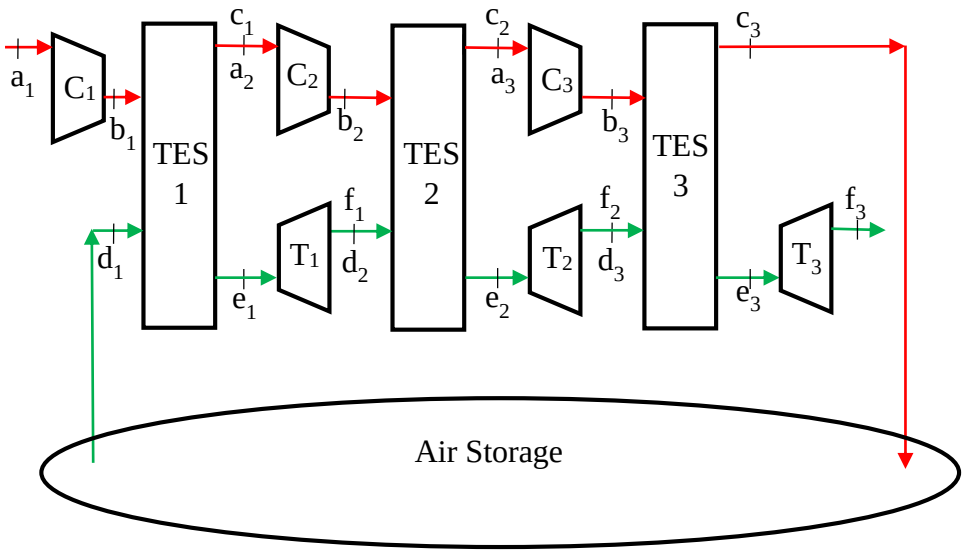

Figure 25. Simple schematic of a three-stage CAES

Operating conditions are presented in Table 17. Once power input, overall pressure ratio and volume of air storage are known, air mass flow rate and charge duration of compression stage and inlet temperature of 1st TES are found.

Table 17. Operating conditions of a 3-Stage CAES

Total Compressor Power Input	$\dot{W}_c$	30	MW
Overall pressure ratio of compressor	r_p	65	-
Number of Stages	n	3	-
Air mass flow rate	$\dot{m}_{air,c}$	61	kg/s
Minimum and maximum operating pressure of air storage	$P_{min} - P_{max}$	40-65	bars
Volume of Cavern	V_{st}	50000	m^3

For the illustrative condition in Table 17, process is estimated to operate about 6.6 hours according to Equation (59). Inlet temperature of the 1st TES is found as 460 K from Equation (32) and mass flow rate of compression stage is 61.4 kg/s from Equation (33). Air properties are taken at 450 K and presented in Table 18.

Table 18. Air properties at 450 K [31]

Density	ρ	0.774	kg/m^3
Constant pressure specific heat	c_p	1021	J/kg-K
Thermal conductivity	k	0.0373	W/m-K
Kinematic viscosity	ν	0.00003239	m^2/s
Prandtl number	Pr	0.686	-

For this operating conditions of CAES, a LHTES and a SHTES are designed and difference of these two TES designs are assessed based on CAES performance.

For these two TES designs, required minimum volume of TESs are used, of which exit temperature reaches inlet temperature at the end of storage duration found as 6.6 hours. Therefore maximum amount of heat is stored and temperature of air and PCMs are at

the maximum temperature. Sizes of the SHTES and LHTES are different because sensible and latent storage show different characteristics.

In SHTES, rock is used as the heat storage medium and $MgCl_2 \cdot 6H_2O$ is used as the heat storage medium of LHTES. Cross sectional area and length of SHTES are 75 m^2 and 10 m and cross sectional area and length of LHTES are 75 m^2 and 7 m. Volume of LHTES is smaller than that of SHTES due to the reasons stated in Section 2.3.1. Number of layers also changes according to the volume of TES tank. Minimum number of layers is selected in a way to obtain an accurate temperature profile inside TES. Number of layers is 5 for SHTES and 4 for LHTES. Length of layers is not exactly same because number of layers becomes non-integer for the same length of TESs.

In Sections 3.4.1 and 3.4.2, change in temperature at the inlet of each TESs, at boundaries of layers in TES and at the exit of each TESs are presented for compression and expansion stages. Positions where temperature is plotted are presented in Figure 26 and Figure 27.

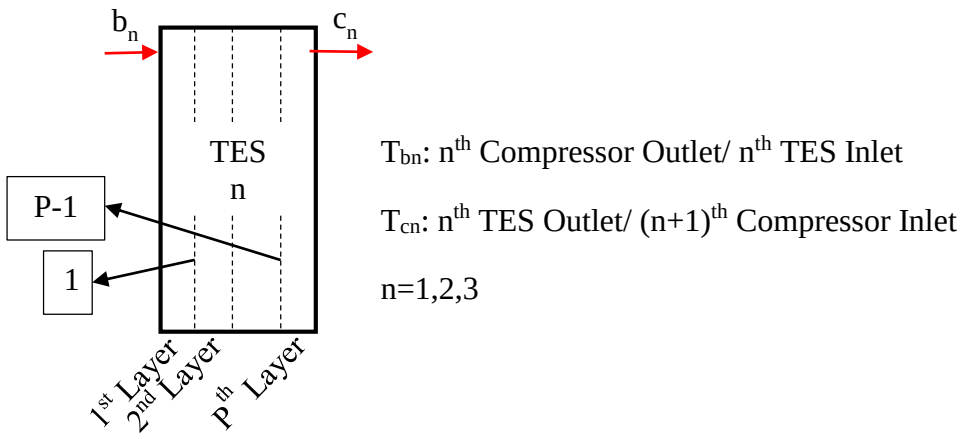

Figure 26. Positions at which temperature distribution is plotted in Sections 3.4.1 and 3.4.2 for compression stage

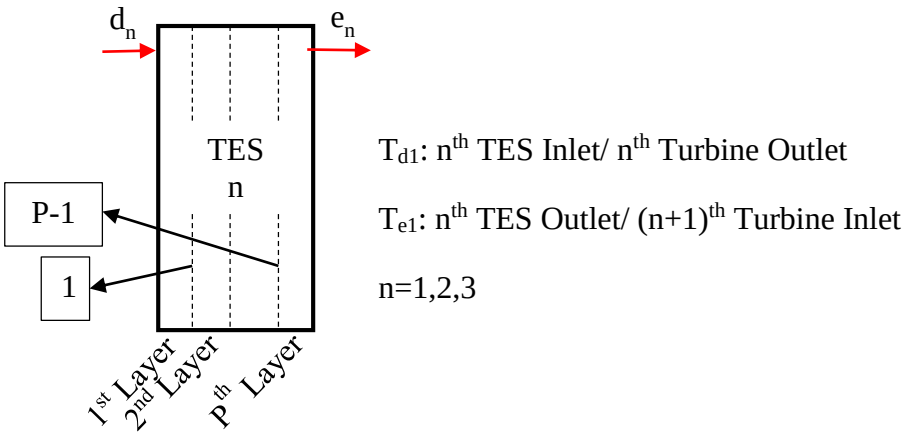

Figure 27. Positions at which temperature distribution is plotted in Sections 3.4.1 and 3.4.2 for expansion stage

For the 1st TES, inlet temperature is the ambient temperature for compression and air storage temperature for expansion.

3.4.1. CAES with SHTES

Cross-sectional area and length of the TES tank filled with rock (SHTES) is 75 m^2 and 10 m. Ambient air is pressurized by the 1st compressor and flows through the 1st TES with 402.1 kPa. Temperature distribution in the 1st TES is presented in Figure 28.

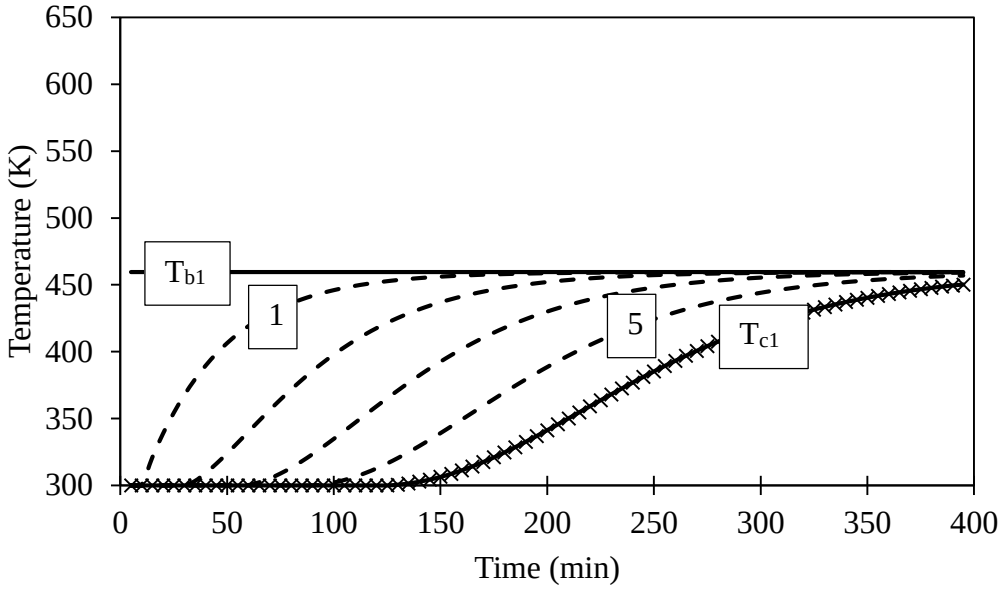

Figure 28. Temperature distribution in the 1st Rock-filled-TES for Case Study

Air leaves the 1st TES and enters 2nd compressor with the pressure drop of 0.7 kPa which can be assumed as negligible. After compressor air pressure is 1613 kPa and air enters to the 2nd TES. In Figure 29, temperature profile in the 2nd TES is presented.

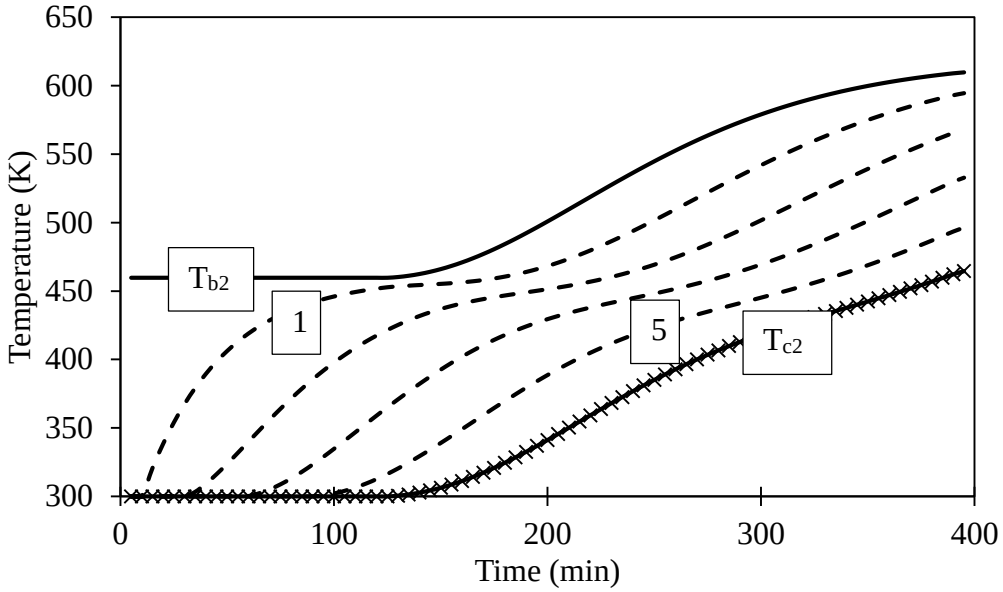

Figure 29. Temperature distribution in the 2nd Rock-filled-TES for Case Study

Temperature profile changes in the 2nd TES due to the variation in the inlet air temperature. Although air temperature at the inlet of 1st TES is constant ambient temperature, temperature at the inlet of the 2nd TES changes with the temperature at the outlet of 1st TES. Therefore air temperature at the exit of 2nd TES exceeds the maximum temperature of the 1st TES, which means that proportion of stored latent heat is different in different TESs.

Third TES is similar to the second TES which is presented in Figure 30.

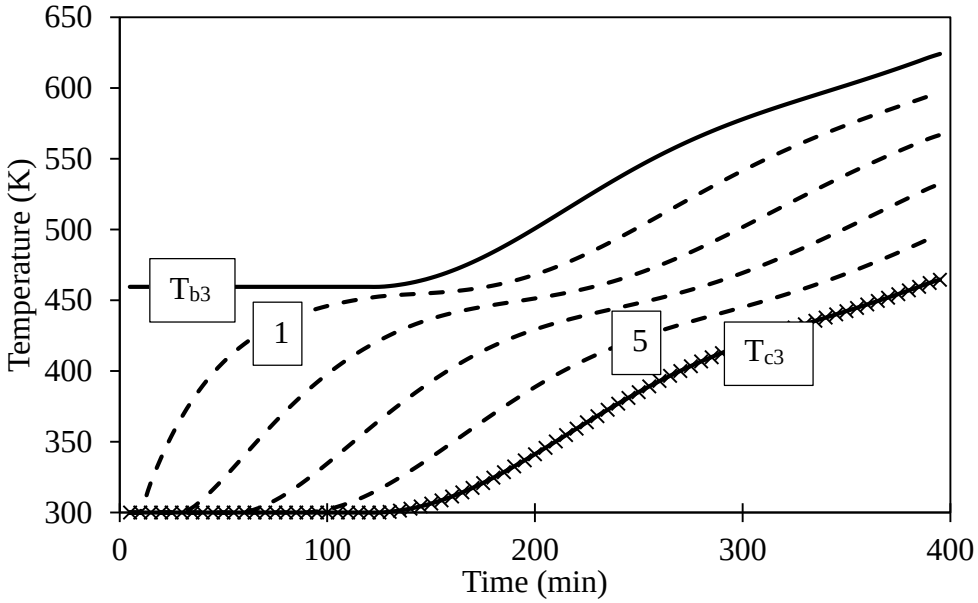

Figure 30. Temperature distribution in the 3rd Rock-filled-TES for Case Study

After 3rd compressor air pressure is 6485.4 kPa, which is close to the desired storage pressure, P_{max} but not same due to the small pressure losses in TESs.

During discharge, compressed air is drawn from the air storage and heated in the 1st TES which is presented in Figure 31.

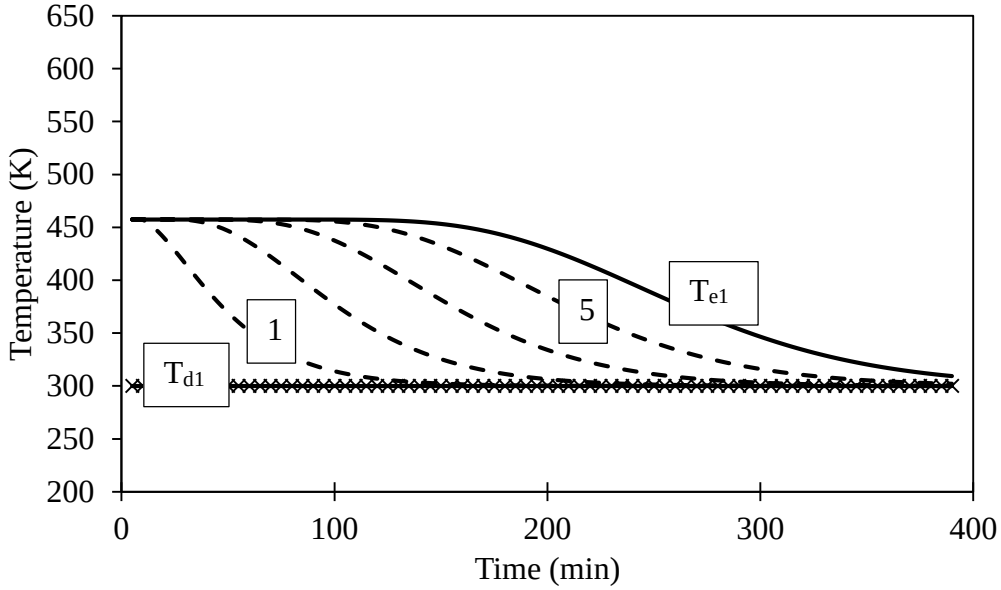

Figure 31. Temperature distribution in the 1st Rock-filled-TES during Discharge for Case Study

At the beginning of the process, air at the outlet of 1st TES remains at the maximum temperature which results in the increase of the power output of turbine. Temperature profile of air inside TES should be as steep as possible to obtain the maximum work output. Then heated air is expanded in the 1st turbine and enters to the 2nd TES. Then, air is expanded two more times in 2nd and 3rd turbines after 2nd and 3rd TESs. Temperature distributions in the TES tanks are presented in Figure 32 and Figure 33.

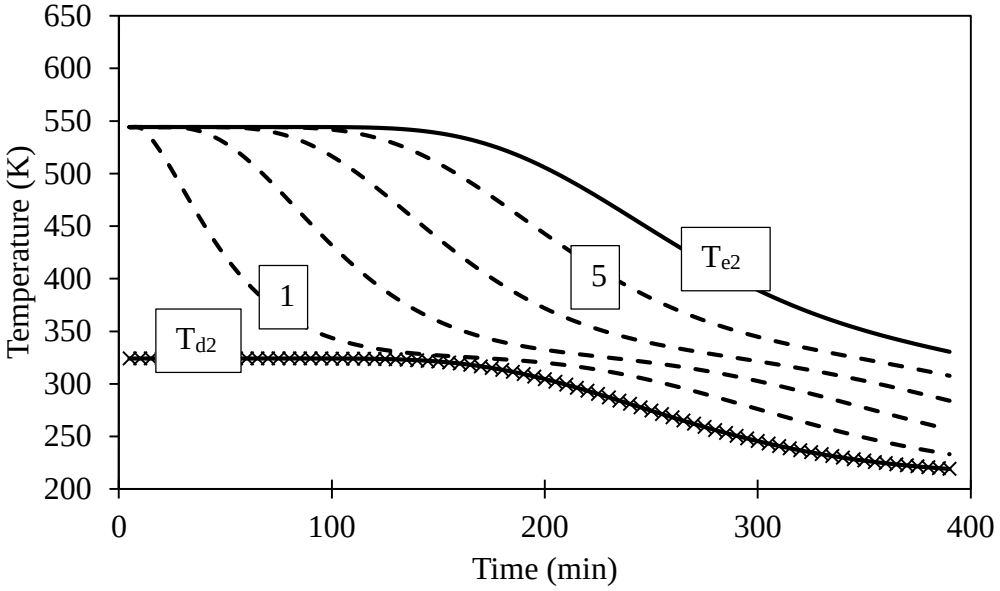

Figure 32. Temperature distribution in the 2nd Rock-filled-TES during discharge for Case Study

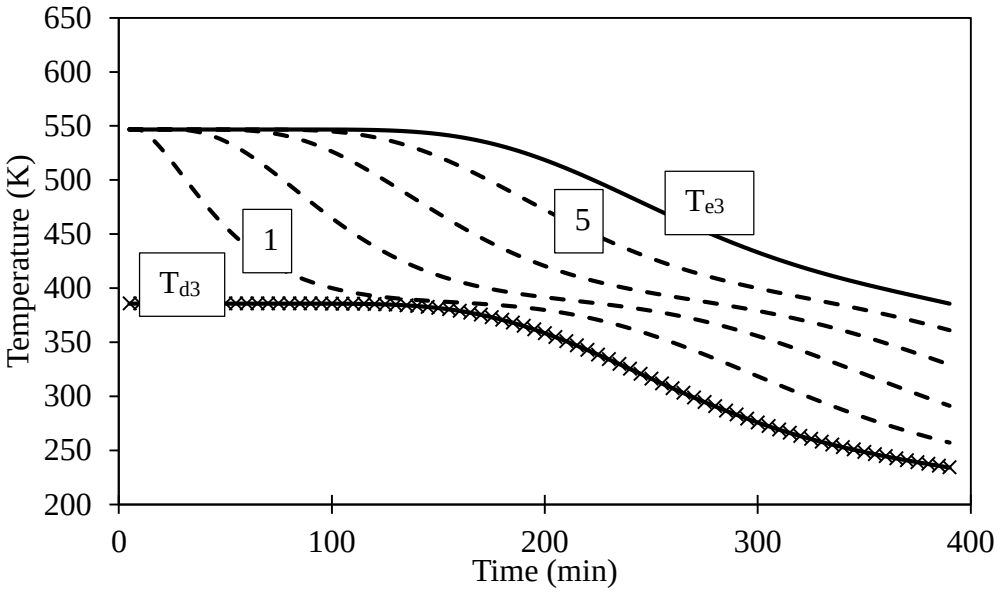

Figure 33. Temperature distribution in the 3rd Rock-filled-TES during discharge for Case Study

In the 2nd and 3rd TESs, temperature decreases to below ambient because previous turbines are fed with low-temperature air. Air at the turbine exhaust can be used to cool air at the compressor inlet.

3.4.2. CAES with LHTES

For the TES filled with $MgCl_2 \cdot 6H_2O$ (LHTES), a tank with cross sectional area and length of 75 m^2 and 7 m is used. The dimensions of LHTES is smaller than those of SHTES because of high heat storage capacity per volume of $MgCl_2 \cdot 6H_2O$. Similar with SHTES, ambient air is compressed to 402.1 kPa and sent to the 1st TES. Temperature profile in the 1st TES is presented in Figure 34.

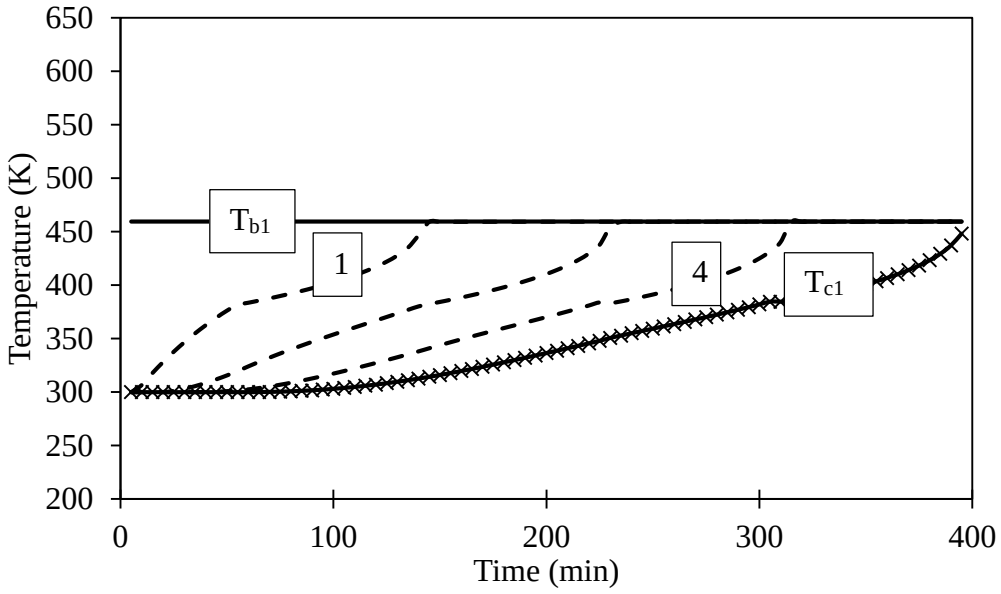

Figure 34. Temperature distribution in the 1st $MgCl_2 \cdot 6H_2O$-filled-TES for Case Study

Pressure loss in LHTES is 0.5 kPa, which is lower than that in SHTES and assumed as negligible similar with SHTES. Reason for the lower pressure loss is the smaller

length of LHTES compared with SHTES. Temperature in the 2nd and 3rd TES tanks is greater than that of 1st because exit temperature of the 1st TES increases unavoidably.

Temperature distribution in the 2nd and 3rd tanks are presented in Figure 35 and Figure 36.

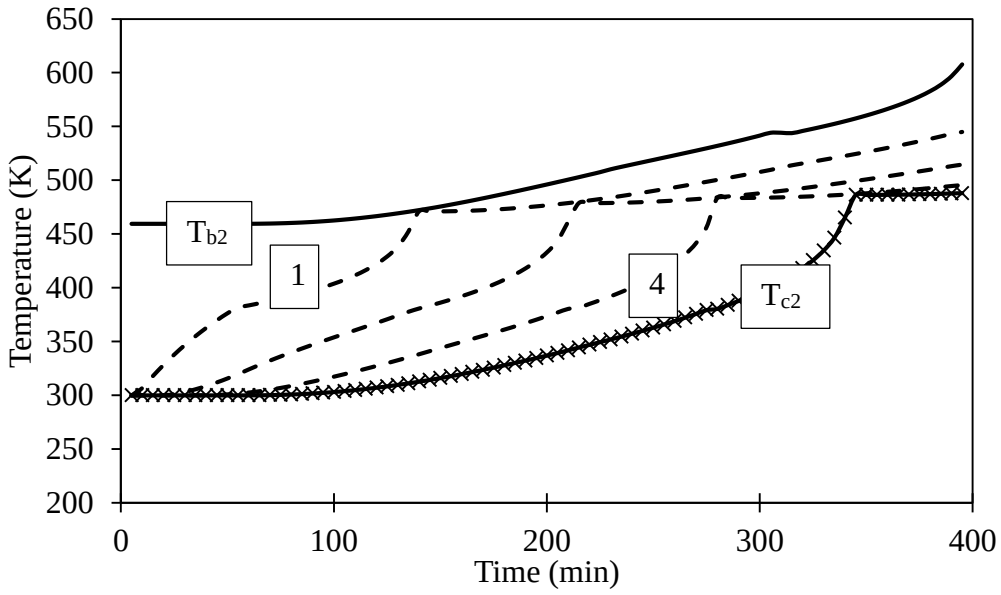

Figure 35. Temperature distribution in the 2nd $MgCl_2 \cdot 6H_2O$-filled-TES for Case Study

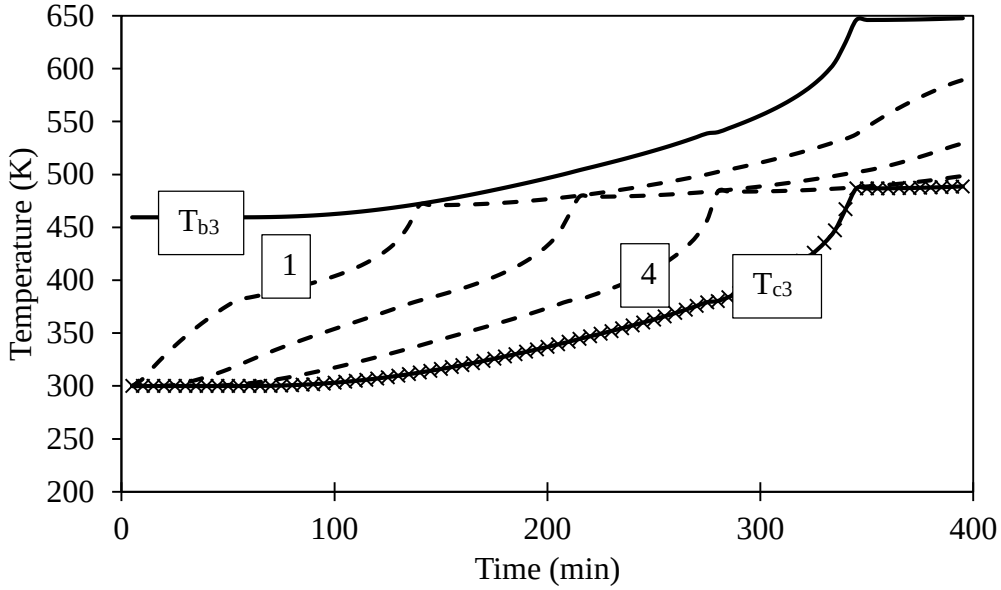

Figure 36. Temperature distribution in the 3rd $MgCl_2 \cdot 6H_2O$-filled-TES for Case Study

After 3rd TES, air is sent to the air storage with the pressure of 6490 kPa, which is slightly higher than air pressure when SHTES is utilized n CAES. For this case, pressure loss is negligible, however, if the

During discharge, compressed air is drawn from air storage and expanded in the 3-stage turbines as heated in TESs. Temperature distributions in TESs are presented in Figure 37-Figure 39.

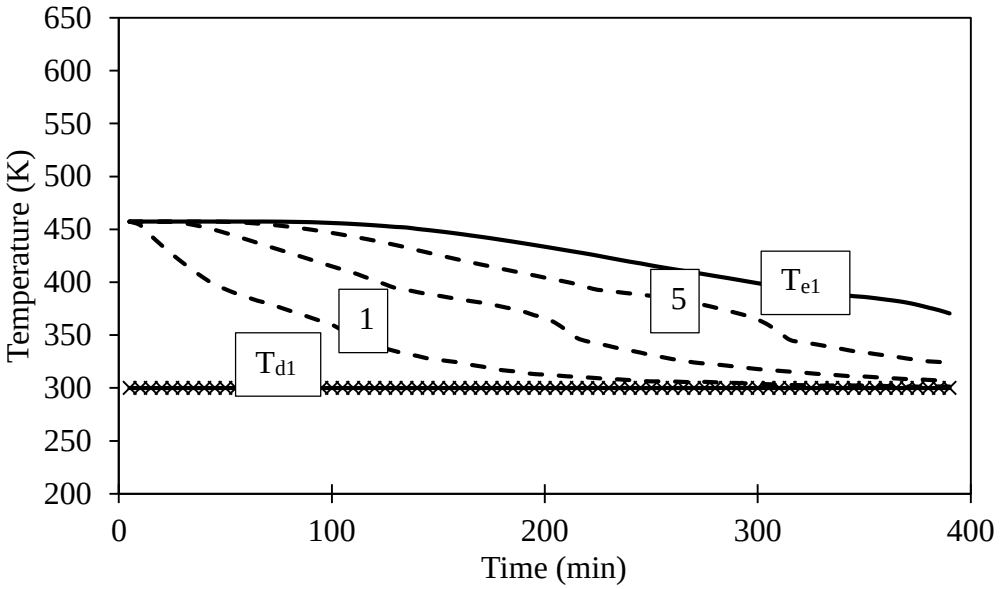

Figure 37. Temperature distribution in the 1st $MgCl_2 \cdot 6H_2O$-filled-TES during discharging for Case Study

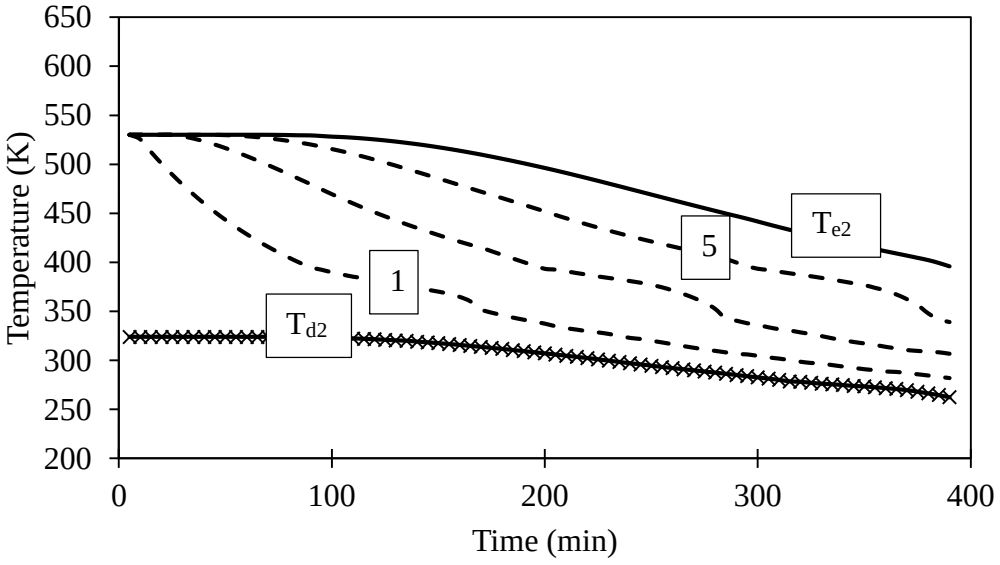

Figure 38. Temperature distribution in the 2nd $MgCl_2 \cdot 6H_2O$-filled-TES for Case Study

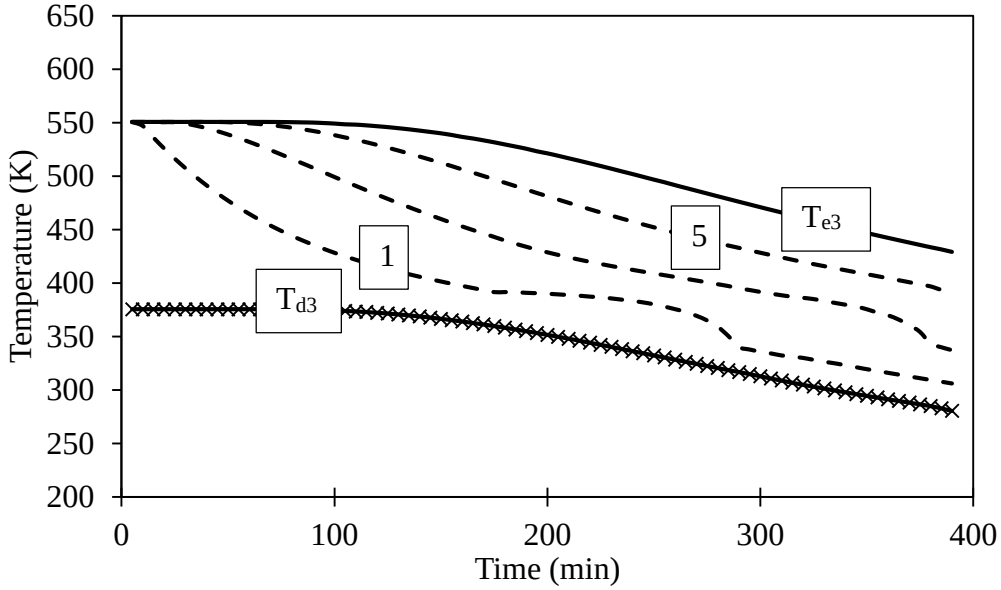

Figure 39. Temperature distribution in the 3rd $MgCl_2 \cdot 6H_2O$-filled-TES for Case Study

In all of the TESs there is a portion of heat which is not discharged. This situation provides more work output in turbines because air temperature at the outlet of TES remains at higher values. On the other hand, the not-discharged heat may cause problem in continuous operation during charging because compressor may be fed by a hot air and compressor may be damaged due to high temperature although continuous operation is not included in this study.

3.4.3. Comparison of TES Tanks filled with Rock and $MgCl_2 \cdot 6H_2O$

For this two TES designs, operating data during charging and can be found in Table 19.

Table 19. Results for the Charge Period of Case Study

Heat Storage Medium	TES Dimensions	W_c (GJ) (x3)	$Q_{tes,\text{charge}}$ (GJ)
Rock	75 m^2 -10 m	237.6	645
$MgCl_2 \cdot 6H_2O$	75 m^2 - 7 m	237.6	624

$MgCl_2 \cdot 6H_2O$ and rock, both operated in the same conditions but $MgCl_2 \cdot 6H_2O$ requires smaller volume. Although stored heat seems small, discharge period is more important. In Table 20, corresponding results for the discharge period are presented.

Table 20. Results for the Discharge Period of Case Study

Heat Storage Medium	$W_{t,1}$ (GJ)	$W_{t,2}$ (GJ)	$W_{t,3}$ (GJ)	$W_{t,1,2,3}$ (GJ)	$Q_{tes,1-2-3}$ (GJ)
Rock	175	204	130	509	667
$MgCl_2 \cdot 6H_2O$	185	210	150	545	709

Round trip efficiency for CAES is defined as the ratio of total work output of turbines to total work input to compressors. Although it is meaningful for real operating conditions, included in this study for comparison. Round trip efficiencies for two systems are 71.4% (Rock-Filled TES + CAES) and 76.5% ($MgCl_2 \cdot 6H_2O$ filled TES + CAES) which are close to each other. However, volume of $MgCl_2 \cdot 6H_2O$ filled tank is 70% of rock filled tank.

3.5. Conclusion

In this chapter, complete model of a CAES system is presented. TES which is modeled in Chapter 2 is implemented in this model. For all the components except TES, only thermodynamic model is used. Detailed analyses of components are not included.

Chapter 3 revealed different characteristics of CAES with TES. For example, if PCMs are used as the heat storage medium, complete heat recovery becomes impossible as discussed in 3.3.1 and also showed in the last two sections of this chapter. With the present study, this can not be eliminated, but as a future work, a different TES system with multiple tanks filled with different materials with different melting temperatures. If the materials are sorted according to their melting temperatures from larger to smaller, during discharge (as PCMs freeze) storage duration would be much smaller and in addition, stored heat and discharged heat would be larger.

Multiple compression and expansion provides high pressure ratios with moderate temperature operation. In this chapter, multiple stage-CAES is analyzed by using different materials as heat storage medium. As expected, $MgCl_2 \cdot 6H_2O$ has a better performance compared to rock. $MgCl_2 \cdot 6H_2O$ filled tank both provides better round-trip efficiency and requires less volume.

CHAPTER 4

CONCLUSION

4.1. Summary

In this thesis, Latent Heat Thermal Energy Storage (LHTES) is designed for Compressed Air Energy Storage (CAES). Although origin of this study is TES design for CAES, different analyses and performance investigation of TES is valid for individual TES designs.

In Chapter 2, mathematical model of LHTES is presented. Transient energy equation is solved by Finite Volume Method with Central Differencing (CD) Explicit Schemes. Spherical PCM capsules are treated as full sphere and spherical wall according to state of PCM, liquid, solid or mixture, and corresponding heat transfer equations are solved in order to obtain temperature of each layer. Melting and freezing of PCM show different characteristics. Although melting is more straightforward, freezing has a stochastic nature which is evaluated with a probability function of freezing. Sensible thermal storage can also be studied with the present model by setting latent heat to zero and melting temperature to a high value. In Chapter 2, parametric studies are conducted in order to evaluate operational characteristics of PCM-filled TES and Rock-filled TES with different dimensions. These designs are compared in terms of stored heat, storage duration and stored heat per storage duration. Heat transfer coefficients and pressure drops for corresponding designs are also presented.

In Chapter 3, remaining components of CAES, compressor, turbine and air storage are designed. These components are modeled thermodynamically and detailed models are not included in the present discussion. Compressor works with fixed compressor power and pressure ratio and exit temperature and mass flow rate are found from the

model. In the present model, volume of air storage is fixed and charging duration is determined by air storage volume, mass flow rate of charging and pressure limits of the air storage. Turbine works with an inlet temperature fixed by TES and variable pressure ratio specified by pressure variation inside air storage. In Chapter 3, effects of different parameters, e.g. TES exit temperature during charging and discharging, and mass flow rates on the system outputs, such as turbine power output are investigated. Finally, an illustrative condition is considered as a case study of a multiple-stage CAES with two different TES system filled with two different PCMs are designed and performances of the two system are compared.

4.2. Future Works

In Chapter 2, supercooling phenomenon is discussed and theory in the existing literature is presented. Numerical analyses about supercooling is limited to water but studies regarding other materials are not observed. For the improvements in LHTES, supercooling should be investigated in detail for PCMs.

In this study, real energy demand and supply profiles are not used but a constant excess electricity is assumed. CAES with LHTES should be modeled for a real case and applicability of this system should be confirmed.

Parametric studies should be extended to a wider range of operating parameters, such as different size ranges may be considered. Small-scale operations may be considered after these parametric study.

4.3. Concluding Remarks

In this thesis, a LHTES is modeled applicable to a CAES. LHTES model provides flexibility of model SHTES therefore LHTES and SHTES could be compared in the present model.

LHTES is demonstrated as better than SHTES in Chapters 2 and 3. This result was expected. LHTES system provide a better storage capacity per unit volume.

Considering charging durations, rock is not affected by change in radius but charging time varies for PCMs for different sizes.

Although the effect of melting temperature is not investigated in detail, there may be an evidence that storage duration may be affected by how close melting temperature is to the operating temperature limits.

Different than SHTES, LHTES may result in different durations in charging and discharging. This phenomenon is presented in Section 2.3.4. The reason for this may be the supercooling because temperature of the liquid phase of PCM decreases below melting point without freezing. Delay of the freezing keeps temperature difference small therefore high heat transfer rate is reached later.

In the present study, air storage is modeled as constant-volume. With a fixed mass flow rate through charging, storage duration is obtained. This approach provides to model real-case problems simply. If a natural cavern is used, charging duration can be estimated. If a small-scale CAES is designed, volume of the air storage tank can be adjusted accordingly.

In the last chapter, a three-stage CAES system is modeled and effects of sensible and latent heat storage materials is investigated. Round-trip efficiencies are close to each other however, there is still stored heat in TESs filled with PCM therefore this heat can be used for other purposes and efficiency increases. On the other hand, TES filled with rock does not have a remaining stored energy. If the stored energy is not used as suggested, this would be a problem because when charging starts the remaining energy from the previous cycle may damage the compressors because air temperature may increase above the limit of safety.

REFERENCES

[1] International Energy Agengy, “2014 Key World Energy STATISTICS,” 2014.

[2] H. Ibrahim, a. Ilinca, and J. Perron, “Energy storage systems-Characteristics and comparisons,” *Renew. Sustain. Energy Rev.*, vol. 12, no. 5, pp. 1221–1250, 2008.

[3] G. Salgi and H. Lund, “System behaviour of compressed-air energy-storage in Denmark with a high penetration of renewable energy sources,” *Appl. Energy*, vol. 85, no. 4, pp. 182–189, 2008.

[4] H. Chen, T. N. Cong, W. Yang, C. Tan, Y. Li, and Y. Ding, “Progress in electrical energy storage system: A critical review,” *Prog. Nat. Sci.*, vol. 19, no. 3, pp. 291–312, Mar. 2009.

[5] A. Sharma, V. V. Tyagi, C. R. Chen, and D. Buddhi, “Review on thermal energy storage with phase change materials and applications,” *Renew. Sustain. Energy Rev.*, vol. 13, pp. 318–345, 2009.

[6] M. S. Whittingham, “History, Evolution, and Future Status of Energy Storage,” *Proc. IEEE*, vol. 100, no. Special Centennial Issue, pp. 1518–1534, 2012.

[7] B. Roberts, “Capturing grid power,” *IEEE Power Energy Mag.*, vol. 7, no. 4, pp. 32–41, 2009.

[8] “Palmiet pumped storage scheme.” [Online]. Available: http://www.eskom.co.za/AboutElectricity/VisitorCentres/Pages/Palmiet_Pumped_Storage_Scheme.aspx.

[9] H. Ibrahim and A. Ilinca, “Techno-Economic Analysis of Different Energy Storage Technologies,” *Energy Storage - Technologies and Applications, Dr. Ahmed Zobaa (Ed.), ISBN: 978-953-51-0951-8, InTech,*. [Online]. Available: http://www.intechopen.com/books/energy-storage-technologies-and-applications/techno-economic-analysis-of-different-energy-storage-technologies.

[10] D. Villela, V. V. Kasinathan, S. De Valle, M. Alvarez, G. Frantziskonis, P. Deymier, and K. Muralidharan, “Compressed-air energy storage systems for

stand-alone off-grid photovoltaic modules," *Conf. Rec. IEEE Photovolt. Spec. Conf.*, pp. 962–967, 2010.

[11] "General Compression." [Online]. Available: http://www.generalcompression.com/.

[12] "SustainX." [Online]. Available: http://www.sustainx.com/.

[13] "LightSail Energy." [Online]. Available: http://www.lightsail.com/.

[14] F. S. Barnes and J. G. Levine, *Large energy storage systems handbook*. 2011.

[15] J. Kondoh, I. Ishii, H. Yamaguchi, a Murata, K. Otani, K. Sakuta, N. Higuchi, S. Sekine, and M. Kamimoto, "Electrical energy storage systems for energy networks," vol. 41, 2000.

[16] S. M. Hasnain, "Review on sustainable thermal energy storage technologies, Part II: cool thermal storage," *Energy Convers. Manag.*, vol. 39, no. 11, pp. 1139–1153, 1998.

[17] Hasnain S.M., "Review on sustainable thermal energy storage technologies, Part I: heat storage materials and techniques," *Energy Convers. Manag.*, vol. 39, no. 11, pp. 1127–1138, 1998.

[18] M. M. Farid, A. M. Khudhair, S. A. K. Razack, and S. Al-Hallaj, "A review on phase change energy storage: Materials and applications," *Energy Convers. Manag.*, vol. 45, pp. 1597–1615, 2004.

[19] B. Zalba, J. M. Marín, L. F. Cabeza, and H. Mehling, *Review on thermal energy storage with phase change: materials, heat transfer analysis and applications*, vol. 23. 2003.

[20] R. W. E. Power, "ADELE – Adiabatic compressed-air energy storage for electricity supply," 2010.

[21] Modern Power Systems, "Adele CAES Pilot." [Online]. Available: http://business.highbeam.com/4364/article-1G1-297718155/adele-caes-pilot-site-selected-but-project-delayed.

[22] S. Zunft, C. Jakiel, M. Koller, and C. Bullough, "Adiabatic Compressed Air Energy Storage for the Grid Integration of Wind Power," no. October, pp. 26–28, 2006.

[23] Y. Zhang, K. Yang, X. Li, and J. Xu, “The thermodynamic effect of thermal energy storage on compressed air energy storage system,” *Renew. Energy*, vol. 50, pp. 227–235, Feb. 2013.

[24] Y. Zhang, K. Yang, X. Li, and J. Xu, “The thermodynamic effect of air storage chamber model on Advanced Adiabatic Compressed Air Energy Storage System,” *Renew. Energy*, vol. 57, pp. 469–478, 2013.

[25] N. Hartmann, O. Vöhringer, C. Kruck, and L. Eltrop, “Simulation and analysis of different adiabatic Compressed Air Energy Storage plant configurations,” *Appl. Energy*, vol. 93, pp. 541–548, 2012.

[26] Y. M. Kim, “Novel concepts of compressed air energy storage and thermo-electric energy storage,” École Polytechnique Fédérale De Lausanne, 2012.

[27] K. Tastankaya, “Development of a methodology for sizing and assessment of wind integrated advanced adiabatic compressed air energy storage system (AA-CAES),” Middle East Technical University, 2014.

[28] F. D. S. Steta, “Fernando De Samaniego Steta,” 2010.

[29] a. F. Regin, S. C. Solanki, and J. S. Saini, “Heat transfer characteristics of thermal energy storage system using PCM capsules: A review,” *Renew. Sustain. Energy Rev.*, vol. 12, pp. 2438–2451, 2008.

[30] H. Hu and S. A. Argyropoulos, “Mathematical modelling of solidification and melting : a review,” vol. 4, pp. 371–396, 1996.

[31] T. L. Bergman, F. P. Incropera, and A. S. Lavine, *Fundamentals of Heat and Mass Transfer*. 2011.

[32] B. Xu, P. W. Li, and C. L. Chan, “Extending the validity of lumped capacitance method for large Biot number in thermal storage application,” *Sol. Energy*, vol. 86, no. 6, pp. 1709–1724, 2012.

[33] J. P. Bédécarrats, J. Castaing-Lasvignottes, F. Strub, and J. P. Dumas, “Study of a phase change energy storage using spherical capsules. Part II: Numerical modelling,” *Energy Convers. Manag.*, vol. 50, no. 10, pp. 2537–2546, 2009.

[34] R. S. Subramanian, “Flow through Packed Beds and Fluidized Beds,” pp. 1–6, 2001.

[35] J.-P. Bedecarrats, “Etude des transformations des matériaux à changement de phase encapsulés déstinés au stockage du froid,” 1993.

[36] S. L. Chen and C. L. Chen, “Effect of nucleation agents on the freezing probability of supercooled water inside capsules,” *ASHRAE Trans.*, vol. 106, no. February 2015, pp. 37–41, 2000.

[37] T. Kousksou, J. P. Bédécarrats, J. P. Dumas, and a. Mimet, “Dynamic modelling of the storage of an encapsulated ice tank,” *Appl. Therm. Eng.*, vol. 25, pp. 1534–1548, 2005.

[38] J. P. Bédécarrats, J. Castaing-Lasvignottes, F. Strub, and J. P. Dumas, “Study of a phase change energy storage using spherical capsules. Part I: Experimental results,” *Energy Convers. Manag.*, vol. 50, no. 10, pp. 2527–2536, 2009.

[39] J. Bedecarrats, F. Strub, B. Falcon, and J. Dumas, “Phase-change thermal energy storage using spherical capsules: performance of a test plant,” *Int. J. Refrig.*, vol. 19, no. 3, pp. 187–196, 1996.

[40] J. C. Choi and S. D. Kim, “Heat transfer in a latent heat-storage system using $MgC1_2*6H_2O$ at the melting point,” *Energy*, vol. 20, no. I, pp. 13–25, 1995.

[41] C. L. Yaws, *Yaws’ Critical Property Data for Chemical Engineers and Chemists*. 2012.

[42] D. Groulx and W. Ogoh, “Solid-Liquid Phase Change Simulation Applied to a Cylindrical Latent Heat Energy Storage System,” 2009.

[43] A. J. Pimm, S. D. Garvey, and M. de Jong, “Design and testing of Energy Bags for underwater compressed air energy storage,” *Energy*, vol. 66, pp. 496–508, 2014.